



CENTER FOR INFRASTRUCTURE ENGINEERING STUDIES

Development and Validation of Steel Reinforced Polymer (SRP) for Strengthening of Transportation

Infrastructures

By

Dr. Paolo Casadei

Dr. Antonio Nanni

Dr. Tim Ibell

University Transportation Center Program at

The University of Missouri-Rolla

**UTC
R94**

Disclaimer

The contents of this report reflect the views of the author(s), who are responsible for the facts and the accuracy of information presented herein. This document is disseminated under the sponsorship of the Department of Transportation, University Transportation Centers Program and the Center for Infrastructure Engineering Studies UTC program at the University of Missouri - Rolla, in the interest of information exchange. The U.S. Government and Center for Infrastructure Engineering Studies assumes no liability for the contents or use thereof.

Technical Report Documentation Page

1. Report No. UTC R94	2. Government Accession No.	3. Recipient's Catalog No.	
4. Title and Subtitle Development and Validation of Steel Reinforced Polymer (SRP) for Strengthening of Transportation Infrastructures		5. Report Date June 2005	
		6. Performing Organization Code	
7. Author/s Dr. Paolo Casadei, Dr. Antonio Nanni, Dr. Tim Ibelle		8. Performing Organization Report No. RG001232 OT094	
9. Performing Organization Name and Address Center for Infrastructure Engineering Studies/UTC program University of Missouri - Rolla 223 Engineering Research Lab Rolla, MO 65409		10. Work Unit No. (TRAIS)	
		11. Contract or Grant No. DTRS98-G-0021	
12. Sponsoring Organization Name and Address U.S. Department of Transportation Research and Special Programs Administration 400 7 th Street, SW Washington, DC 20590-0001		13. Type of Report and Period Covered Final	
		14. Sponsoring Agency Code	
15. Supplementary Notes			
<p>16. Abstract</p> <p>This report presents the characterization, laboratory and field validation of steel reinforced polymer (SRP) and steel reinforced grout (SRG) strengthening materials for strengthening of transportation infrastructures. These new composite materials consist of steel cords formed by interwoven steel wires embedded within a polymer resin or cementitious grout matrix. The properties of SRP are evaluated experimentally and compared to micromechanical equations to determine a suitability of these equations for the prediction of material constants. Laboratory tests were undertaken on shallow reinforced concrete beams strengthened with SRP and SRG materials and comparing experimental results to identical reinforced concrete beams strengthened with fiber reinforced polymer, with equal amount of strengthening. All beams were tested in a four point bending configuration, constantly monitoring deflections, strain and crack width opening. A type of anchor system to retard complete peeling of SRP/SRG laminates have been investigated and results of its performance are presented. Based upon the promising results of the two previous test campaigns, a series of tests on prestressed concrete double-T real-scale beams strengthened with SRP materials have been undertaken. The in-situ test campaign was made possible, due to the demolition of an existing concrete structure. Tests consisted in a control beam, a beam strengthened with one ply of SRP and a third and last beam strengthened with two plies of SRP and by anchoring at both ends the plies with SRP U-wraps. All beams were tested in a three point load configuration and were monitored at midspan for deflections as well as strains in the composite material.</p>			
17. Key Words ductility; flexure; in-situ load test; polymer; prestressed concrete; reinforced concrete; steel reinforced polymer; strengthening	18. Distribution Statement No restrictions. This document is available to the public through the National Technical Information Service, Springfield, Virginia 22161.		
19. Security Classification (of this report) unclassified	20. Security Classification (of this page) unclassified	21. No. Of Pages	22. Price

DEVELOPMENT AND VALIDATION OF STEEL REINFORCED POLYMER (SRP) FOR STRENGTHENING OF TRANSPORTATION INFRASTRUCTURES

EXECUTIVE SUMMARY

This report presents the characterization, laboratory and field validation of steel reinforced polymer (SRP) and steel reinforced grout (SRG) strengthening materials for strengthening of transportation infrastructures.

These new composite materials consist of steel cords formed by interwoven steel wires embedded within a polymer resin or cementitious grout matrix. The properties of SRP are evaluated experimentally and compared to micromechanical equations to determine a suitability of these equations for the prediction of material constants.

Laboratory tests were undertaken on shallow reinforced concrete beams strengthened with SRP and SRG materials and comparing experimental results to identical reinforced concrete beams strengthened with fiber reinforced polymer, with equal amount of strengthening. All beams were tested in a four point bending configuration, constantly monitoring deflections, strain and crack width opening. A type of anchor system to retard complete peeling of SRP/SRG laminates have been investigated and results of its performance are presented.

Based upon the promising results of the two previous test campaigns, a series of tests on prestressed concrete double-T real-scale beams strengthened with SRP materials have been undertaken. The in-situ test campaign was made possible, due to the demolition of an existing concrete structure. Tests consisted in a control beam, a beam strengthened with one ply of SRP and a third and last beam strengthened with two plies of SRP and by anchoring at both ends the plies with SRP U-wraps. All beams were tested in a three point load configuration and were monitored at midspan for deflections as well as strains in the composite material.

The report presents a summary of all three experimental campaigns.

ACKNOWLEDGMENTS

The project was sponsored by the Industry/University Cooperative Research Center on Repair of Buildings and Bridges (RB2C) at the University of Missouri – Rolla (UMR), and the University Transportation Center (UTC) at UMR. Hardwire LLC., Pocomoke City, MD, provided the steel tapes for all three projects, Sika Corporation, Lyndhurst, NJ, and Mapei Spa, Milan, Italy, the resins and Structural Preservation Systems, Hanover, MD, for the onsite support and installation of SRP material.

1 TABLE OF CONTENTS

1	TABLE OF CONTENTS.....	III
	LIST OF FIGURES	IV
2	LIST OF TABLES	V
	NOTATIONS.....	VI
3	INTRODUCTION	- 8 -
3.1	Background.....	- 8 -
3.2	Objectives	- 11 -
3.3	Methodology.....	- 11 -
4	MATERIAL CHARACTERIZATION	- 12 -
4.1	Introduction.....	- 12 -
4.2	Experimental Analysis.....	- 12 -
4.2.1	Evaluation of Material Constants of SRP	- 12 -
4.3	Comparison of Experimental Results with Predictions Obtained by Micromechanical Theory.....	- 17 -
4.4	Experimental Evaluation of Flexural Properties of SRP	- 20 -
4.5	Conclusions.....	- 21 -
5	LABORATORY TESTING.....	- 22 -
5.1	Introduction.....	- 22 -
5.2	Experimental Program	- 22 -
5.3	Test Program Design.....	- 24 -
5.3.1	Design material properties	- 24 -
5.3.2	Upgrade strategy	- 26 -
5.4	Specimen Preparation	- 29 -
5.5	Instrumentation	- 30 -
5.6	Test Results.....	- 30 -
5.7	Discussion	- 35 -
5.8	Conclusions.....	- 39 -
6	FIELD TESTING.....	- 42 -
6.1	Introduction.....	- 42 -
6.2	Experimental Program	- 42 -
6.2.1	Building Characteristics.....	- 42 -
6.2.2	Specimens and Installation of Steel Reinforced Polymer.....	- 44 -
6.2.3	Test Setup and Instrumentation	- 46 -
6.2.4	On-Site Safety.....	- 48 -
6.3	Results and Discussion	- 48 -
6.4	Analytical approach	- 52 -
6.5	Conclusions.....	- 55 -
7	REFERENCES	- 56 -

LIST OF FIGURES

Figure 1 – Microscope View of Cord Cross section.....	- 9 -
Figure 2 – Examples of Cords with Different Filament Twisting	- 9 -
Figure 3 – Example of Medium Density Tape of Old Generation	- 10 -
Figure 4 - Example of Medium Density Tape of New Generation.....	- 11 -
Figure 5 -	- 13 -
Figure 6 - Typical Stress-Strain Relationship of SRP Tapes	- 25 -
Figure 7 - Geometry and Reinforcement of Strengthened Beams (dimension in mm)	- 28 -
Figure 8 - Nail Anchors	- 29 -
Figure 9 - Load-Deflection Curves: Control vs. 3X2 Bonded Beams	- 31 -
Figure 10 - Load-Deflection Curves: Control vs. 12X Bonded Beams	- 31 -
Figure 11 - Load-Deflection Curves: Control vs. FRP Bonded Beams.....	- 32 -
Figure 12 - Lateral View of Failure of A-2 Beam	- 33 -
Figure 13 - Bottom View of Failure of A-2 Beam	- 33 -
Figure 14 - Bottom View of Failure of B-1 Beam.....	- 33 -
Figure 15 - Bottom View of Failure of B-2 Beam.....	- 33 -
Figure 16 - Nail Bearing in Beam B-3.....	- 34 -
Figure 17– Bloomington Parking Garage.....	- 42 -
Figure 18 – Double-T Geometry Details (<i>SI units 1 mm = 0.039 in</i>).....	- 43 -
Figure 19 – Test Beams (<i>SI units 1 mm = 0.039 in</i>).....	- 44 -
Figure 20 – SRP Laminate Stress vs Strain Behavior.....	- 45 -
Figure 21 – SRP Installation Procedure.....	- 46 -
Figure 22 – Test Set Up	- 47 -
Figure 23 – Installed Instrumentation.....	- 48 -
Figure 24 – Load vs Mid-Span Deflection (<i>Beam DT-C</i>).....	- 49 -
Figure 25 – Load vs Mid-Span Deflection (<i>Beam DT-1</i>)	- 49 -
Figure 26 – Load vs Mid-Span Deflection (<i>Beam DT-2U</i>)	- 49 -
Figure 27 – Load vs Mid-Span Strain (<i>Beam DT-1</i>).....	- 49 -
Figure 28 – Load vs Mid-Span Strain (<i>Beam DT-2U</i>).....	- 49 -
Figure 29 – Failure Mechanisms in Strengthened Beams	- 50 -
Figure 30 – Strain and Stress Distribution Across Beam Depth.....	- 53 -

2 LIST OF TABLES

Table 1 - Properties of Epon 828 with Hardener HT-386	- 12 -
Table 2 - Specimens Used in Experiments	- 13 -
Table 3 - Results of Longitudinal Tension Tests	- 14 -
Table 4 - Results of Longitudinal Compression Tests.....	- 14 -
Table 5 - Results of Transverse Tension Tests	- 15 -
Table 6 - Results of Transverse Compression Tests.....	- 16 -
Table 7 - Results of Tensile Tests Conducted with	- 16 -
Table 8 - Comparison of Mechanical Properties Obtained Experimentally to Theoretical Predictions Based on Micromechanics	- 19 -
Table 9 - Specimens Used in Flexural Tests.....	- 20 -
Table 10 - Results of Flexural Tests: Flexural Strength	- 21 -
Table 11 - Test Matrix and Summary of Experimental Results	- 23 -
Table 12 - Mechanical Properties of Epoxy Matrix.....	- 24 -
Table 13 - Properties of Steel Cords	- 25 -
Table 14 - Mechanical Properties of Cementitious Grout	- 26 -
Table 15 - Properties of Construction Materials.....	- 43 -
Table 16 - Mechanical Properties of Epoxy Resin	- 45 -
Table 17 - Material Properties of Steel Tape	- 45 -
Table 18 - Beam Test Results	- 48 -
Table 19 - Analytical Beam Results at Ultimate	- 54 -

NOTATIONS

A_{SRP}	:	$n(t_{SRP} w_{SRP})$ area of SRP reinforcement [mm ²]
A_{pB}	:	area of bottom steel tendon reinforcement [mm ²]
A_{pT}	:	area of top steel tendon reinforcement [mm ²]
c	:	depth of the neutral axis [mm]
E_{SRP}	:	$\frac{f_{fu_SRP}}{\varepsilon_{fu_SRP}}$ tensile modulus of elasticity of SRP [MPa]
E_c	:	$4700\sqrt{f'_c}$ tensile modulus of elasticity of concrete (ACI 318 Section 8.5.1) [MPa]
d_{pB}	:	depth of bottom steel tendon [mm]
d_{pT}	:	depth of top steel tendon [mm]
f'_c	:	ultimate compressive strength of concrete [MPa]
f_{fe_SRP}	:	effective stress in the SRP; stress level attained at section failure [MPa]
f_{fu_SRP}	:	$\overline{f_{fu_SRP}} - 3\sigma$ ultimate design tensile strength in the SRP [MPa]
$\overline{f_{fu_SRP}}$:	mean ultimate tensile strength of SRP based upon a population of tests as per ASTM D 3039 [MPa]
f_{pB}	:	stress in bottom steel tendon at ultimate [MPa]
f_{pT}	:	stress in top steel tendon at ultimate [MPa]
h	:	height of the cross section [mm]
t_{SRP}	:	nominal thickness of one ply of SRP reinforcement [mm]
w_{SRP}	:	width of one ply of SRP [mm]
ε_c	:	strain level in the concrete [mm/mm]
ε'_c	:	$\frac{1.71f'_c}{E_c}$ ultimate compressive strain of concrete (Todeschini et al. 1998) [mm/mm]
ε_{fu_SRP}	:	$\overline{\varepsilon_{fu_SRP}} - 3\sigma$ design rupture strain in the SRP [mm/mm]
$\overline{\varepsilon_{fu_SRP}}$:	mean rupture strain of SRP based upon a population of tests as per ASTM D 3039 [mm/mm]
β_1	:	$2 - \frac{4[(\varepsilon_c/\varepsilon'_c) - \tan^{-1}(\varepsilon_c/\varepsilon'_c)]}{(\varepsilon_c/\varepsilon'_c)\ln(1 + \varepsilon_c^2/\varepsilon_c'^2)}$ ratio of the depth of the equivalent rectangular stress block to the depth of the neutral axis (Todeschini et al. 1998)
γ	:	$\frac{0.9\ln\left(1 + \frac{\varepsilon_c^2}{\varepsilon_c'^2}\right)}{\beta_1 \frac{\varepsilon_c}{\varepsilon'_c}}$ multiplier on f'_c to determine the intensity of an equivalent rectangular stress distribution for concrete (Todeschini et al. 1998)

k_m : Bond dependent coefficient for flexure

3 INTRODUCTION

3.1 Background

The use of advanced composite materials in the construction industry is nowadays a mainstream technology (Rizkalla and Nanni 2003), supported by design guidelines such as the ACI 440.2R-02 (2002) in the United States and the Fib-Bulletin 14 (2001) in Europe. Fiber reinforced polymer (FRP) composite materials, even though very attractive, may be hindered by lack of ductility and fire resistance. Both issues are currently under study by the research community (Williams et al. 2004, Bisby et al. 2004, Seible et al. 1997), in order to provide on one hand, better knowledge in terms of overall structural performance and, on the other, remedies such as coatings that could prolong fire resistance.

A new family of composite materials based on unidirectional high strength twisted steel wires (about 7 times stronger than typical common reinforcing bars) of fine diameter ($0.20\sim 0.35\text{ mm}$ ($0.0079\sim 0.0138\text{ in}$)), that can be impregnated with thermo-set (referred to as steel reinforced polymer, SRP) or cementitious (referred to as steel reinforced grout, SRG) resin systems is studied in this report. SRP/G has the potential to address the two shortcomings mentioned for FRP, in fact: a) steel cords have some inherent ductility; and b) impregnation with cementitious paste may overcome the problems of fire endurance and lowering down the application cost considerably.

The steel cords used in SRP are identical to those used for making the reinforcement of automotive tires, and manufactured to obtain the shape of the fabric tape prior to impregnation. The steel cords produced for steel reinforced composites are manufactured by Goodyear Tire and Rubber Company, Asheboro, NC and remanufactured and distributed by Hardwire, LLC, Pocomoke City, Maryland (www.hardwirellc.com).

Steel reinforced polymers (SRP) are less expensive composites that are currently considered for numerous applications in civil engineering, such as bridge and building repair. A cross section of such cord photographed under a microscope is depicted in Figure 1.

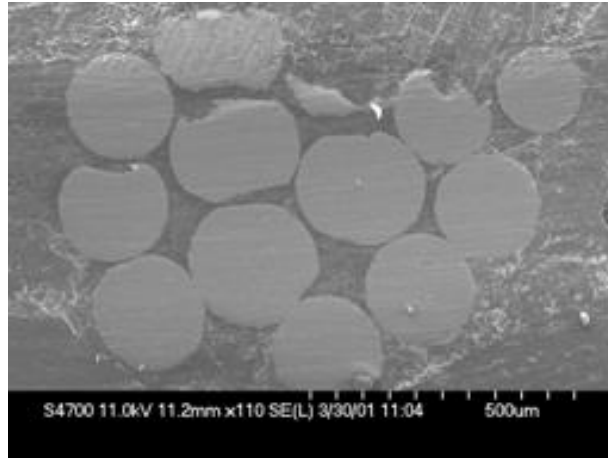
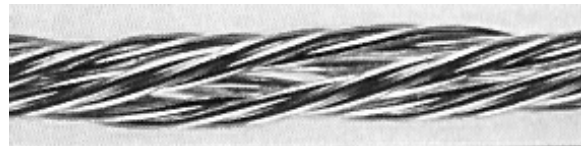


Figure 1 – Microscope View of Cord Cross section

Performance of a composite material utilizing steel wires is controlled by the stress transfer between the wires and the matrix. A single high-strength wire may be deficient due to low interfacial shear strength and stiffness. This problem is solved in SRP by using twisted steel filaments forming the cord, as shown in Figure 2*a* and Figure 2*b*.



a) 12 Wires Wrapped by 1 Wire



b) 3 Cords of 2-Wire Each Twisted Around

Figure 2 – Examples of Cords with Different Filament Twisting

The rough surface of the cord provides a mechanical interlock with the matrix resulting in a system suitable for structural applications. As an example, the cord shown in Figure 2*a* is produced by twisting one wire at a short lay length around 12 wires that are twisted in a long lay length. The wrap wire provides additional surface roughness and tightens the cord enhancing its integrity. The cord shown in Figure 2*b* consists of a two-wire strand twisted around a three-wire strand. Differently from the sample in Figure 2*a*, this cord has a more pronounced surface roughness distribution.

The stiffness and strength of composites utilizing the steel cords shown in Figure 2*a* and Figure 2*b* may differ due to a different cord surface geometry. In all cases, it is desirable to produce SRP where the failure of the cord under tension preempts its pullout.

Unidirectional cords can be held in place by knit yarns forming an appropriate pattern of fabric. The yarns control the spacing of the cords and as a result, the “net” behaves like a fabric that can be stretched or bent, without losing its integrity. A typical knit yarn material is polyester; a “net” consisting of the cords held by polyester yarns is shown in Figure 3*a*. The addition of copper knit yarns results in the fabric capable of maintaining the spacing between steel cords, even under significant handling loads. In addition, such fabric has excellent electric conductivity. Copper wires used in this example had a diameter equal to 0.006 in. The copper wire is tied to the steel cords by the spiraling polyester knit thread, as shown in Figure 3*b*.

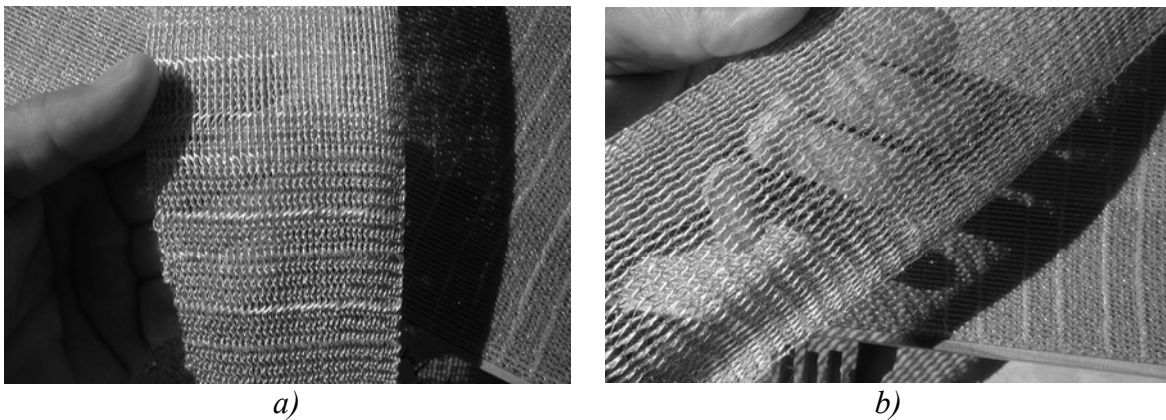
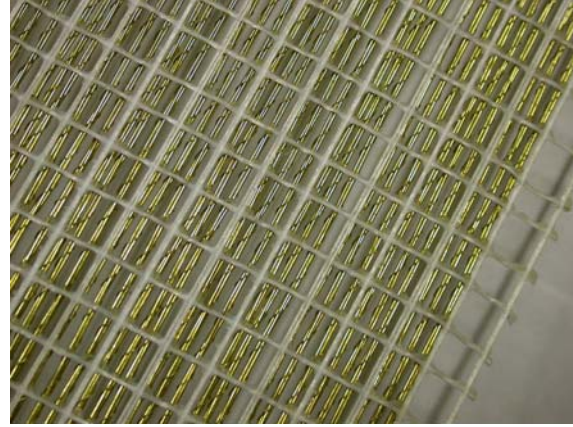


Figure 3 – Example of Medium Density Tape of Old Generation

Post-testing enhancements have been made to the fabric making process that no longer require knitting of materials and simply bind the steel cords to a fiberglass scrim with adhesives. This allows for better control of cord density during the manufacturing process and makes possible the manufacture of any density fabric. The process also yields a 17% increase in the number of cords per inch and thus higher fabric properties. The new fabric lays flatter and straighter than the knitted fabrics and can be applied faster and easier (see Figure 4). Additionally, new cord designs have been created to optimize the compressive qualities and provide more balanced compressive and tensile properties.



a) Front view of Tape with Cords Held Together by a Polyester Scrim



b) Back view of Tape with detail of Polyester Scrim

Figure 4 - Example of Medium Density Tape of New Generation

3.2 Objectives

The scope of this project is the evaluation of performance through laboratory and field testing of a new type of strengthening material for upgrading the infrastructures, based on high strength steel filament cords to be impregnated with either cementitious or epoxy matrices.

3.3 Methodology

To evaluate the performance of such new kind of strengthening material, studies have been undertaken to firstly characterize the mechanical properties of each single components (matrix and fibers), secondly laboratories studies have compared the performance of reinforced concrete beams strengthened with the new material and compared with others strengthened with well established strengthening materials such as fiber reinforced polymers. Ultimately field testing of real scale structures have been performed to validate the findings of previous research studies.

4 MATERIAL CHARACTERIZATION

4.1 Introduction

4.2 Experimental Analysis

Steel cords employed in the present study had a diameter equal to 0.044 in and consisted of 13 filaments (Figure 2a). Three of these filaments had a diameter equal to 0.22 micron, nine filaments had 0.20-micron diameter, and one of them had a 0.15-micron diameter. Several different impregnating resins were considered, including Epon 828 + Hardener HT-386, M-Brace Saturant, SikaDur 330 and SikaTop 121. Epon 828 was used in the tests described in the report.

4.2.1 Evaluation of Material Constants of SRP

Unidirectional SRP samples were tested in tension and compression using an MTS 880 testing machine. The specimens were pre-manufactured using compression molding into a plate, shipped to the laboratory, and cut to size by waterjet.

The matrix material used in the tested specimens was Epon 828 with Hardener HT-386. The properties of Epon 828 tested after curing at 200°F for two hours are outlined in Table 1. These properties were used in the computations performed to compare micromechanical predictions for material properties with experimental data.

Table 1 - Properties of Epon 828 with Hardener HT-386

Specimen code	E_m (ksi)	ν_m	Strength (psi)	G_m (ksi)
sp1	471	0.350	7163	175
sp2	460	0.380	8527	167
sp3	439	0.362	7460	161
sp4	408	0.341	7947	152
Average	444	0.358	7774	164

The specimens had geometrical dimensions as reported in Table 2 together with the direction of the load as compared to that of the cords. A photograph depicting the cross section of a typical specimen is shown in Figure 5.



Figure 5 -

Table 2 - Specimens Used in Experiments

Specimen Code	Angle of Load-to-Cords Direction (deg)	Width (in)	Length (in)	Thickness (in)	Test Type
SLT1-5	0	1.0	12.0	0.25	Tension
STT1-5	90	1.0	7.0	0.25	Transverse Tension
STC1-5	90	0.5	5.5	0.25	Transverse Compression
SLC1-1	0	0.5	5.5	0.25	Compression
S45_1-3	45	1.0	10.0	0.25	Tension (For shear modulus)

The results of the tests are shown in Table 3 through Table 7. In these tables, the subscripts “w,” “c” and “cs” refer to steel wire, steel cord and SRP composite, respectively. The directions 1 and 2 refer to the longitudinal (along the cord) and transverse (perpendicular to the cord) directions. The material constants that are analyzed include the elastic moduli (E_1, E_2), the shear modulus (G_{12}), and the Poisson ratios (ν_{12}, ν_{21}). In addition, the strength of the material (F) is evaluated, both in tension and in compression, in the longitudinal and transverse directions. The results of longitudinal tensile testing of five specimens are presented in Table 3. In particular, longitudinal tensile moduli of individual wires and the cord are shown in this table. Predictably,

the modulus of the cord is smaller than that of wires, as a result of the twisting and matrix content in the cord (the latter is clearly visible in Figure 1).

Table 3 - Results of Longitudinal Tension Tests

Specimen code	E_{1c} (Msi)	E_{1w} (Msi)	E_{1cs} (Msi)	v₁₂	F_c (ksi)	F_w (ksi)	F_{cs} (ksi)	Notes
SLT1-1	19.5	25.4	6.8	0.273	319	417	112	
SLT1-2	23.3	30.5	8.1	0.329	342	447	118	
SLT1-3	22.0	28.8	7.8	0.409	276	361	98	Failure at grip
SLT1-4	23.2	30.4	8.3	0.373	343	449	123	
SLT1-5	23.0	30.1	8.4	0.468	340	445	124	
Average	22.2	29.0	7.9	0.370	324	423.8	115	
Average w/o SLT3					336	440	119	
Average w/o SLT1 and SLT3	22.9	29.9	8.2	0.395	342	447	122	

The longitudinal modulus of SRP is much lower than the corresponding modulus of the cords. The variation in the stiffness of five tested specimens was not very large, except for the SLT1-1. The reason for this difference is evident from the comparison of the stiffness of the constituent wires of the specimens. Obviously, the specimen in question was manufactured using substandard steel wires, compared to its counterparts. The same conclusion follows from the comparison of the strength of wires used in SLT1-1 and other specimens (except for SLT1-3). Accordingly, the results for SLT1-1 are discounted in the average values shown in the last row of the table.

Table 4 - Results of Longitudinal Compression Tests

Specimen Code	E_{1c} (Msi)	E_{1w} (Msi)	E_{1cs} (Msi)	v₁₂
SLC1	34.4	45.0	12.0	0.407
SLC2	33.3	43.6	12.0	0.246
SLC3	27.8	36.4	9.8	0.427
SLC4	36.6	47.9	12.6	0.468
Average	32.6	42.6	11.4	0.387

Table 5 - Results of Transverse Tension Tests

Specimen Code	E₂ (Msi)	v₂₁	Strength (psi)
STT1	1.19	0.065	2354
STT2	0.74	0.045	2178
STT3	0.58	0.040	2193
STT4	0.83	0.034	2178
STT5	0.91	0.050	2193
Average	0.85	0.047	2219

As indicated in the Table 3, the specimen SLT1-3 failed at grips. Therefore, the failure stress obtained for this specimen is not included in the calculation of the strength of SRP. Accordingly, the average value in the last row of the table include the stiffness and Poisson ratio evaluated from the analysis of specimens SLT1-2 through 5 and the strength from the analysis of specimens SLT1-2, 4 and 5.

The results of longitudinal compressive tests are shown in Table 4. Notably, the stiffness (modulus) of SRP in compression is much higher than in tension. This is explained by a much higher compressive stiffness of the wires that constitute the cords (compare Table 3 and Table 4). The results for compressive strength are not shown in Table 4 since the mode of failure observed in the experiments was cord buckling. Again, post-testing enhancements to the cord design have addressed the cord buckling failure by creating a structure that resists this type of failure by eliminating the deformations in the core filaments which result from the cord manufacturing process.

The results of transverse tension and transverse compression tests are collected in Table 5 and Table 6. Predictably, the transverse stiffness and strength in tension are much lower than in compression. A significant difference in the Poisson ratios ν_{21} evaluated in transverse tests under tensile and compressive loads was also observed. Note that the ratio of the Poisson value in tension to its counterpart in compression is close to being inversely proportional to the ratio of the stiffness in tension to that in compression.

Table 6 - Results of Transverse Compression Tests

Specimen code	E_2 (Msi)	ν_{21}	Strength (psi)
STC1	0.86	0.042	-8693
STC2	1.65	0.037	-9012
STC3	0.93	0.026	-10356
STC4	0.77	0.033	-9620
STC5	1.97	0.023	-8389
Average	1.24	0.032	-9214

The in-plane shear modulus G_{12} was obtained by combining the results from the tension tests in longitudinal and transverse directions with the results from the tests on coupons oriented at 45° relative to the applied tensile load. The transformation equation for the stiffness of a lamina oriented at an angle θ relative to the applied load is

$$\frac{1}{E_\theta} = \frac{\cos^4 \theta}{E_1} + \frac{\sin^4 \theta}{E_2} + \left(\frac{1}{G_{12}} - \frac{2\nu_{12}}{E_1} \right) \sin^2 \theta \cos^2 \theta \quad (1.1)$$

From this equation, the shear modulus can be obtained in the form ($\theta = 45^\circ$):

$$G_{12} = \frac{1}{\frac{4}{E_{45}} - \frac{1}{E_1} - \frac{1}{E_2} + \frac{2\nu_{12}}{E_1}} \quad (1.2)$$

The results of these tests are shown in Table 7. Remarkably, the variation between three evaluated specimens was small.

Table 7 - Results of Tensile Tests Conducted with Loading Oriented at 45° Relative to the Cords

Specimen code	E_{45} (Msi)	G_{12} (Msi)
S45_1	0.90	0.31
S45_2	0.95	0.33
S45_3	0.92	0.32
Average	0.92	0.32

4.3 Comparison of Experimental Results with Predictions Obtained by Micromechanical Theory

This comparison is needed to conclude whether it is possible to use micromechanical theories developed for conventional composites to predict the properties of SRP. The applicability of conventional micromechanics may be affected by a number of factors that include relatively large diameter of the cords, twisting of the wires in the cords, and even more importantly, the roughness of cord-matrix interface. Unavoidable porosity of SRP, particularly along the cord-matrix interface with its rough surface, may contribute to the inaccuracy of micromechanical relationships. In this paper, a comparison was made to the micromechanical theory developed based on the mechanics of materials (Gibson 1994). The relationships employed in this theory are outlined below.

The assumptions regarding the material phases constituting the composite that are utilized in the micromechanical theory based on mechanics of materials are:

- Both fibers and matrix are linearly elastic isotropic materials.
- Fibers are uniformly distributed in the matrix.
- Fibers are perfectly aligned.
- There is perfect bonding between fibers and matrix.
- The composite lamina is free of voids.

Based on these assumptions, the longitudinal modulus is calculated by the rule of mixtures as:

$$E_1 = E_f V_f + E_m V_m \quad (1.3)$$

where E_1 is a longitudinal elastic modulus of the composite material, E_f is the elastic modulus of the fibers, V_f is the fiber volume fraction (equal to 0.27 in this case), E_m is the elastic modulus of matrix (equal to 0.44 Msi in this case), and V_m is the volume fraction of matrix. The porosity was not measured in the experiments and accordingly, the matrix volume fraction was assumed equal to 0.73. It is necessary to emphasize that the “fibers” referred to in this section represent steel wires, rather than the cords since the latter include the pockets of matrix. Accordingly, the properties of the wires should be employed in the corresponding equations.

The transverse elastic modulus in the direction perpendicular to the fibers can be obtained from the inverse rule of mixtures:

$$E_2 = \frac{E_f E_m}{E_f V_m + E_m V_f} \quad (1.4)$$

The Poisson ratios are determined from:

$$\begin{aligned} \nu_{12} &= \nu_f V_f + \nu_m V_m \\ \nu_{21} &= \frac{E_2}{E_1} \nu_{12} \end{aligned} \quad (1.5)$$

where ν_f is the fiber (steel wires) Poisson's ratio that was equal to 0.30 and ν_m is Poisson's ratio of matrix.

The in-plane shear modulus is obtained from:

$$G_{12} = \frac{G_f G_m}{G_f V_m + G_m V_f} \quad (1.6)$$

where G_f and G_m are the shear moduli of the fiber and matrix materials, respectively.

It is known that the formulae of mechanics of materials are often inaccurate for the transverse modulus of elasticity and for the in-plane shear modulus. The so-called improved mechanics of materials approach (Gibson 1994) results in the following equations for these material constants:

$$\begin{aligned} E_2 &= \frac{E_m}{1 - \sqrt{V_f} (1 - E_m / E_f)} \\ G_{12} &= \frac{G_m}{1 - \sqrt{V_f} (1 - G_m / G_f)} \end{aligned} \quad (1.7)$$

The comparison between experimental results and the properties predicted by micromechanics based on mechanics of materials is presented in Table 8. As follows from this table, theoretical predictions for the tensile and compressive longitudinal modulus of elasticity and for the in-plane shear modulus are in good agreement with experimental data. The agreement for tensile transverse modulus of elasticity and for both Poisson ratios is less satisfactory. However, even

these material constants can be adequately predicted by the micromechanical theory considered in the paper. However, the compressive modulus could not be obtained from micromechanics. Notably, tensile transverse and in-plane shear moduli should be calculated by the improved mechanics of materials, i.e. Eq. (1.7).

The main application of SRP is envisioned in the situations where these composites are subject to longitudinal tension. Accordingly, it is also important to compare the longitudinal strengths available from the experiments (122 ksi) to the theoretically predicted value. The latter value is obtained by the rule of mixtures:

$$F_{cs} = F_f V_f + F_m M_m \quad (1.8)$$

Table 8 - Comparison of Mechanical Properties Obtained Experimentally to Theoretical Predictions Based on Micromechanics

	Experimental Results	Analytical Results	Analytical Results 2*
E_1 (ksi) Tension	8159	8397	
E_1 (ksi) Compression	11400	11826	
E_2 (ksi) Tension	849	605	910
E_2 (ksi) Compression	1240	606	914
ν_{12} Tension	0.395	0.342	
ν_{12} Compression	0.380	0.342	
ν_{21} Tension	0.047	0.041	
ν_{21} Compression	0.032	0.026	
G_{12} (ksi)	320	223	336

Note: * Analytical Results 2 were obtained from the *improved mechanics of materials*.

The results for the in-plane shear modulus were identical in tension and compression.

The substitution of the strengths of wire and matrix yields the value of 126 ksi that is remarkably close to the experimental result. This figure can be further improved by increasing the packing density of the cords (available with the new manufacturing process) and by moving to one of the higher property cords.

4.4 Experimental Evaluation of Flexural Properties of SRP

The flexural strength of SRP was evaluated from a three-point bending test designed according to ASTM D 790. Accordingly, detailed description of the tests is omitted since it can be found in this standard.

Table 9 - Specimens Used in Flexural Tests

Specimen Code	Thickness (in)	Width (in)	Span (in)	Actual Span (in)	Testing Crosshead Rate (in/min)
SF1	0.193	0.652	3.2	3.202	0.0886
SF2	0.170	0.707	3.2	3.202	0.1002
SF3	0.189	0.769	3.2	3.202	0.0903
SF4	0.182	0.732	6.2	6.196	0.3520
SF5	0.182	0.639	6.2	6.196	0.3520

The size of the specimens used in the flexural tests is shown in Table 9. The modes of failure were rupture on the tensile surface of the specimens and fiber microbuckling on their compressed surface. The effect of these modes of failure, particularly fiber microbuckling and related softening of the response, is clearly observed in Fig. 7.

According to ASTM D 790, the maximum flexural stress in the outer fibers at the midspan of the specimen was calculated from:

$$\sigma_f = \frac{3PL}{2bd^2} \quad (1.9)$$

where P is the load, L is the span, and b and d are the width and the depth of the beam, respectively.

In the case of large span-to-depth ratios, such as in specimens SF4 and SF5, the moment at the midspan is affected by relatively large deflections. Accordingly, Eq. (1.9) is modified to account for these effects:

$$\sigma_f = \frac{3PL}{2bd^2} \left[1 + 6 \left(\frac{D}{L} \right)^2 - 4 \left(\frac{d}{L} \right) \left(\frac{D}{L} \right) \right] \quad (1.10)$$

The test results and the corresponding maximum flexural stress (flexural strength) of the tested specimens are shown in Table 10. Note that the difference between flexural strengths found for five specimens was small.

Table 10 - Results of Flexural Tests: Flexural Strength

Specimen Code	Span (in)	Deflection at Max Load (in)	Max Load (lb)	Max Flexural Stress (ksi)	Adjusted Flexural Strength (ksi)
SF1	3.2	0.172	508	100.8	100.8
SF2	3.2	0.199	433	101.4	101.4
SF3	3.2	0.235	630	110.1	110.1
SF4	6.2	0.767	247	95.2	102.6
SF5	6.2	0.501	201	88.2	90.8
Average					101.1

4.5 Conclusions

The research study conducted so far yielded the following conclusions.

- SRP and SRG can be easily and economically manufactured offering great potential for strengthening of concrete bridges and buildings. SRP and SRG elements can be easily and reliably bonded to concrete structures.
- The properties of SRP can be accurately predicted by mechanics of materials using micromechanics models. These properties include the tensile and compressive moduli in the direction of the steel cords, the in-plane shear modulus, and the tensile axial strength. The transverse tensile modulus and the Poisson ratios can also be estimated analytically, though with a smaller accuracy. However, the transverse modulus corresponding to compression could not be accurately determined from micromechanics.

5 LABORATORY TESTING

5.1 Introduction

In order to investigate the flexural behavior of reinforced concrete (RC) beams strengthened with SRP composites, two different types of steel tape with medium and high densities, respectively, were used to strengthen seven RC beams using cementitious grout and epoxy resin and tested to failure under a quasi-static loading. Arrays of nail anchors were used on two of these beams to fasten the steel tape adhered with cementitious grout in order to prevent peeling. Two additional RC beams strengthened with a comparable amount of uni-directional carbon FRP (CFRP) laminates were tested and compared with those strengthened with SRP composites.

5.2 Experimental Program

A total of eleven RC shallow beams, 400 x 200 x 3700 mm in size, were cast. The stirrups were 8-mm diameter steel bars spaced at 100 mm center-to-center. For all specimens, two 8-mm diameter steel bars were used as compression reinforcement. Five 18-mm diameter bars were used as tensile reinforcement for the reference beam (Beam U) (Table 11); for the remaining ten, a deficiency in steel reinforcement area (due for example to a construction or design error, or to structural deterioration) was simulated by using five 10-mm diameter steel bars as tensile reinforcement. Apart from a second beam left as a control specimen (Beam D), the potential of emerging strengthening techniques was assessed by upgrading the nine remaining beams using two different types of steel tape, namely 3X2 cord (Type "A") and 12X cord (Type "B"), and CFRP laminates (Type "C") (Table 11).

All beams were tested as simply supported members, over a clear span of 3.40 m. They were loaded up to failure under a four-point configuration, with a constant moment region of 1.0 m across the mid-span. The load was applied through a 500 kN hydraulic actuator and the test was carried out under displacement control.

Table 11 - Test Matrix and Summary of Experimental Results

Specimen type	Tension steel	External reforc.	Impreg. matrix	No. of Plies [§]	Axial stiff. ratio S	Equiv. reinf. ratio, ρ_{eq} (%)	F_{uth} (kN)	Experimental results					
								F_{cr} (kN)	δ_{cr} (mm)	F_y (kN)	δ_y (mm)	F_u (kN)	δ_u (mm)
U	5 Φ 18	--	---	--	--	1.87	136.1	13.6	1.7	141.4	35.7	147.6	57.1
D	5 Φ 10	--	---	--	--	0.58	47.7	9.2	2.5	43.3	25.1	49.3	102.1
A-1	5 Φ 10	Z-3X2	Epoxy	1	0.16	0.66	85.3	20.7	5.9	60.3	27.1	86.3	75.7
A-2	5 Φ 10	Z-3X2	Epoxy	1	0.32	0.74	110.5	20.8	4.5	79.7	29.9	121.1	72.4
A-3	5 Φ 10	Z-3X2	Epoxy	2	0.32	0.74	107.8	20.1	5.87	76.5	31.5	100.4	54.5
B-1	5 Φ 10	B-12X	Epoxy	1	0.14	0.65	80.4	10.1	1.4	60.4	31.2	88.6	89.2
B-2	5 Φ 10	B-12X	Cement.	1	0.14	0.65	80.4	10.6	1.8	60.0	33.6	72.7	56.8
B-3 *	5 Φ 10	B-12X	Cement.	1	0.14	0.65	80.4	11.5	1.8	57.1	29.9	71.5	60.4
B-4 *	5 Φ 10	B-12X	Cement.	2	0.28	0.72	105.7	9.2	1.3	75.2	34.2	86.7	46.5
C-1	5 Φ 10	Carbon	Epoxy	2	0.21	0.69	96.1	13.8	1.9	75.7	31.4	96.5	55.7
C-2	5 Φ 10	Carbon	Epoxy	3	0.42	0.79	121.0	15.6	2.4	108.6	37.0	134.8	55.8

Note: * with anchor nails; [§] Ply width indicated in Figure 7

5.3 Test Program Design

5.3.1 Design material properties

For the traditional materials, the design properties were assumed equal to 30 MPa for the concrete compressive strength and 500 MPa for the yield strength of the reinforcing steel bars.

The carbon fiber ply is a unidirectional fiber system with a density of 300 g/m². The equivalent fiber thickness is 0.167 mm. According to the manufacturer, the ultimate strength and modulus of elasticity related to fiber volume are 3,450 MPa and 230 GPa, respectively (Mapei 2000). The epoxy used to impregnate the dry carbon fibers was a two-component, medium viscosity, gelatinous solvent-free adhesive (Mapei 2000). Table 12 shows the technical data of the epoxy provided by the manufacturer.

Table 12 - Mechanical Properties of Epoxy Matrix

Matrix	Tensile Strength, MPa	Elongation, % (Strain at failure)	Flexural Modulus MPa
SRP-Epoxy	30	1.5	3800
CFRP-Epoxy	30	1.2	3800

For the steel cord strengthening material, a more detailed discussion follows. The 3x2 steel cord (Hardwire 2002) is made by twisting 5 individual zinc coated wires together – 3 straight filaments wrapped by 2 filaments at a high twist angle. The density of the 3X2 tape used in this research program consists of 87 cords per mm, which is considered high-density tape. The 12X steel cord (Hardwire 2002) is made by twisting two different individual brass coated wires together in 12 strands and then over-twisting one wire around the bundle. The ridge provided by the wrap wire works to share load into the matrix and tighten the cord during the tensile loading. The density of the 12X tape consisted of 6.3 cords per cm, which is considered medium-density tape. Table 13 summarizes the geometrical and mechanical (tensile strength, f_{tu} ; ultimate rupture strain, e_{fu} ; and tensile modulus of elasticity, E_f) properties of the steel cords.

Table 13 - Properties of Steel Cords

Description	Cord Coating	Filament Diameter (mm)	Cord Area (mm ²)	Cords per cm	f _{tu} (MPa)	ε _{tu} (mm/mm)	E _f (GPa)
Z-3X2	Zinc	3 - 0.35, 2 - 0.35	0.48	8.7	3070	0.017	184
B-12X	Brass	3 - 0.22, 9 - 0.20	0.43	6.3			

A typical stress-strain curve of SRP tapes is depicted in Figure 6 where it is shown that this material behaves linearly to failure. Experimental tests have shown that the non-linear behavior is negligible and there is practically no yielding of the steel. The stress-strain relationship of Figure 6 was used for design.

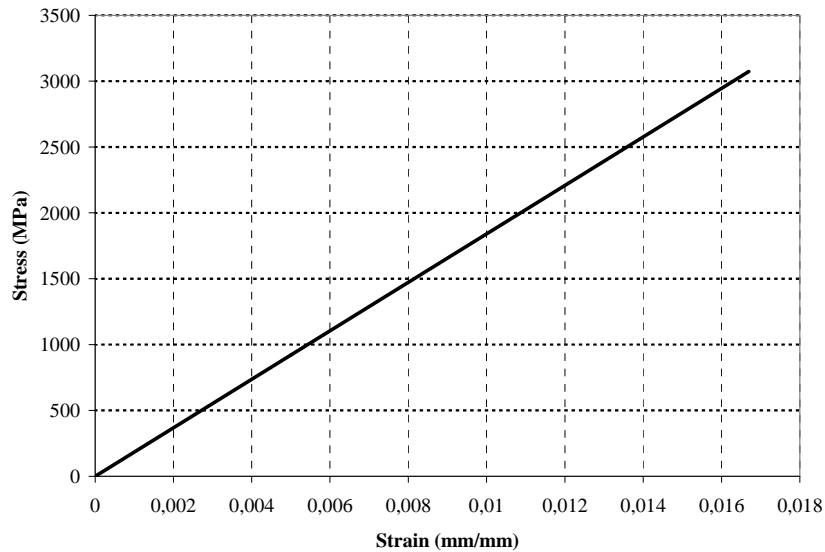


Figure 6 - Typical Stress-Strain Relationship of SRP Tapes

A high-performance two-component 100% solid epoxy resin (Sika 2005) was used to impregnate and bond the steel tape to the concrete substrate. The technical data of the epoxy resin, supplied by the manufacturer, are shown in Table 12. The cementitious grout (Sika 2005) used to bond the steel tape was a two-component, polymer-modified, pore sealing mortar with the additional benefit of a penetrating corrosion inhibitor. It has a finishing time of 45 to 60 min. depending on temperature and relative humidity. The technical data of the cementitious grout, supplied by the manufacturer, are shown in Table 14.

Table 14 - Mechanical Properties of Cementitious Grout

Matrix	*Flexural Strength, MPa	*Compression Strength, MPa	*Splitting Tensile Strength, MPa	*Bonding Strength, MPa
Cementitious grout	13.8	41.4	5.2	13.8

* Strength at 28th day

5.3.2 Upgrade strategy

The nominal flexural strength of Beams U and D was computed according to the ACI 318-02 recommendations without reduction factors; for the remaining specimens strengthened with either SRP or CFRP, the theoretical calculations were conducted according to the ACI 440.2R-02 guidelines.

As for the strengthening strategy, the design of Beam C-1 was performed in order to double the capacity of the control specimen, Beam D; then, the strengthening of Beam C-2 aimed at attaining a flexural strength similar to that of control specimen Beam U by doubling the CFRP area installed on C-1. In order to carry out the strengthened beam design, the following parameters were established (Table 11):

- The axial stiffness ratio $S: E_{ext}A_{ext}/E_sA_s$ (being E_{ext} and A_{ext} , and E_s and A_s the elastic modulus and the total area of externally bonded composites and internal steel bars, respectively); and
- The equivalent reinforcement ratio $\rho_{eq}=\rho_s+\rho_{ext}(E_{ext}/E_s)=\rho_s(1+S)$ (being ρ_s and ρ_{ext} the reinforcement ratios of A_s and A_{ext} over the concrete cross sectional area computed as width of the cross section times the depth of the internal reinforcement)

The amount of SRP to be installed on seven specimens was such to provide values of ρ_{eq} similar to that of specimens C-1 or C-2. Once the SRP layout was determined with this criterion, the flexural strength of each SRP-strengthened specimen was calculated assuming that ACI 440.2R-02 procedure could be extended to this technology.

Table 11 reports the test matrix of the research program, summarizing the area of internal tensile steel, the type and matrix of the externally bonded reinforcement, the number of plies, and the values of both the S and ρ_{eq} ratios. Considering the adopted test setup, the ultimate load, F_{uth} ,

corresponding to the predicted flexural capacity of each beam was computed and reported in the next column of Table 11. Figure 7 shows geometric details for all strengthened beams. Seven beams were bonded with steel tapes impregnated with epoxy resin or cementitious grout (A and B beams); the remaining two beams (C-1 and C-2) were strengthened with CFRP laminates using epoxy resin. Two of the beams strengthened with steel tape and cementitious grout were mechanically anchored with nail anchors (B-3 and B-4). The nail anchor selected for this application was a wide ringed head nylon anchor with zinc plated hammer screw (Figure 8). The anchor is 6 mm in diameter and 60 mm long. A 24 mm diameter washer was used to enlarge the ringed head of the anchor in order to obtain a better hold to the SRP.

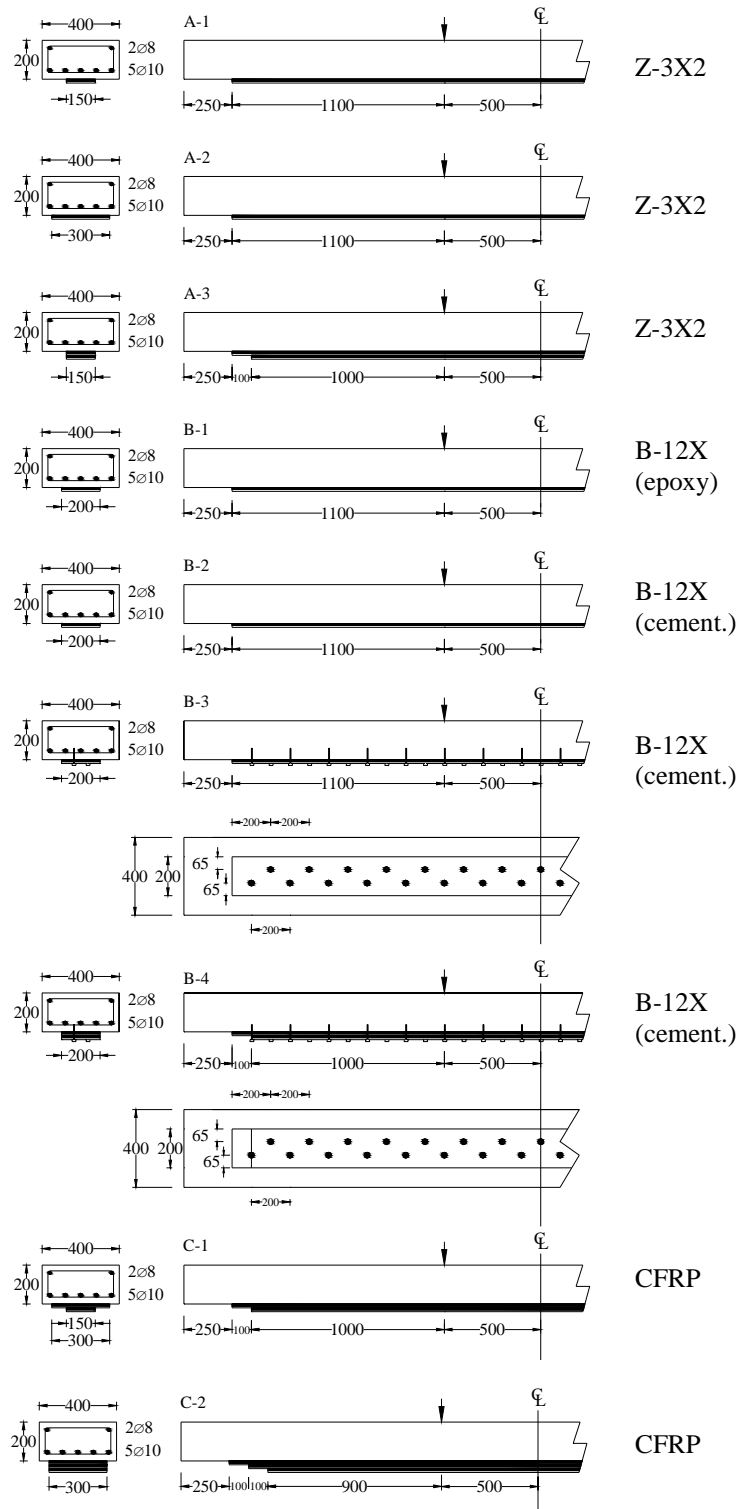


Figure 7 - Geometry and Reinforcement of Strengthened Beams (dimension in mm)

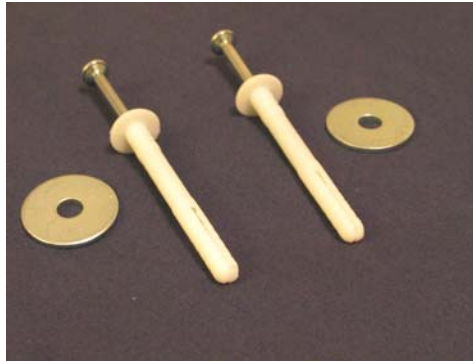


Figure 8 - Nail Anchors

5.4 Specimen Preparation

The bottom face of all beams was sandblasted and cleaned to ensure proper bond before strengthening. No primer was used for bonding SRP tapes with either epoxy or cementitious grout. When a uniform and complete mixing of the epoxy was observed, it was spread to areas where the steel tape had contact. The steel tape was cut to design length, and pressed onto the wet epoxy gel with a hard roller. Where two plies of steel tape were used, an additional layer of epoxy was spread and the previously mentioned steps were repeated. The second ply started 10 cm from the cut-off point of the first ply.

For beams bonded with cementitious grout, the same installation procedure was followed. For beams anchored with nail anchors, a total of 31 holes, 60 mm deep and 6 mm in diameter, were drilled alternatively along two parallel lines, with a center-to-center distance of 200 mm (see Figure 7) prior to strengthening. After bonding the steel tape with cementitious grout, the anchors were hammered into the holes and locked in with 24 mm diameter washers.

The procedure for applying the CFRP laminates was as recommended by the manufacturer (Mapei 2000); suggestions provided by ACI 440.2R-02 (2002) guidelines for externally bonded FRP systems were also considered. The surface preparation started with a layer of primer followed by a layer of putty. After the putty had hardened, the carbon fiber sheet was adhered to the surface with the epoxy; then steps similar to those used for the installation of SRP were followed.

5.5 Instrumentation

All beams were instrumented to record global and local parameters. The mid-span deflection was measured by a vertical linear variable displacement transducer (LVDT). Three horizontal LVDTs were placed on one side of the specimen to record displacements over a length of 0.35 m across the mid-span at depth of 5 mm, 55 mm and 175 mm from the compressive fiber, respectively. On the opposite side, crack width and concrete shortening were measured using demec targets placed 50 mm center-to-center on a total length of 0.55 m at the same depth of the LVDTs on the other side of the beam. Readings were taken at selected load levels. A total of 20 strain gages were used during each test to measure strains on the externally bonded reinforcement. Depending on width and number of plies, the strain gage arrangement slightly changed for each beam. In general, some gages were placed within the constant moment region and some at the cut-off points; longitudinal and transverse strain profiles were obtained.

5.6 Test Results

Before testing the beam specimens, characteristics of the traditional materials were verified and found to be consistent with the design assumption. Concrete cubes (with side of 150 mm) showed an average compressive strength of about 40.1 MPa. For the reinforcing steel bars (three samples per diameter) average values of 500 MPa, 600 MPa and 12% were found for the yield strength, the ultimate strength and the ultimate strain, respectively.

The load-mid-span deflection curves of tested beams are depicted in Figure 9 through Figure 11, which show the trends of each group of beams strengthened with same material systems compared to the two unstrengthened beams. Values of loads and mid-span deflections at first cracking (F_{cr} and δ_{cr}), yielding of tensile steel bars (F_y and δ_y) and ultimate (F_u and δ_u) are summarized in Table 11. First cracking of beam U occurred at a load of 13.6 kN, while Beam D showed the first crack at a load of about 9.2 kN. After first cracking, a loss of stiffness occurred for both beams; curves highlight a change in slope which is more significant for beam D than for U (Figure 9). The shapes of the load deflection curves indicate another loss of stiffness at loads of 141.4 kN and 43.3 kN for Beam U and D, respectively. This is due to yielding of the tensile reinforcement that occurred at mid-span deflections of 35.7 mm and 25.1 mm, respectively. After these thresholds, the behavior of both beams was characterized by large flexural cracks and

then collapse due to concrete crushing in the constant moment region. Failure loads were equal to 147.6 kN and 49.3 kN for Specimens U and D; their ultimate behavior was characterized by a ductility factor δ_u/δ_y of 1.6 and 4.0, respectively.

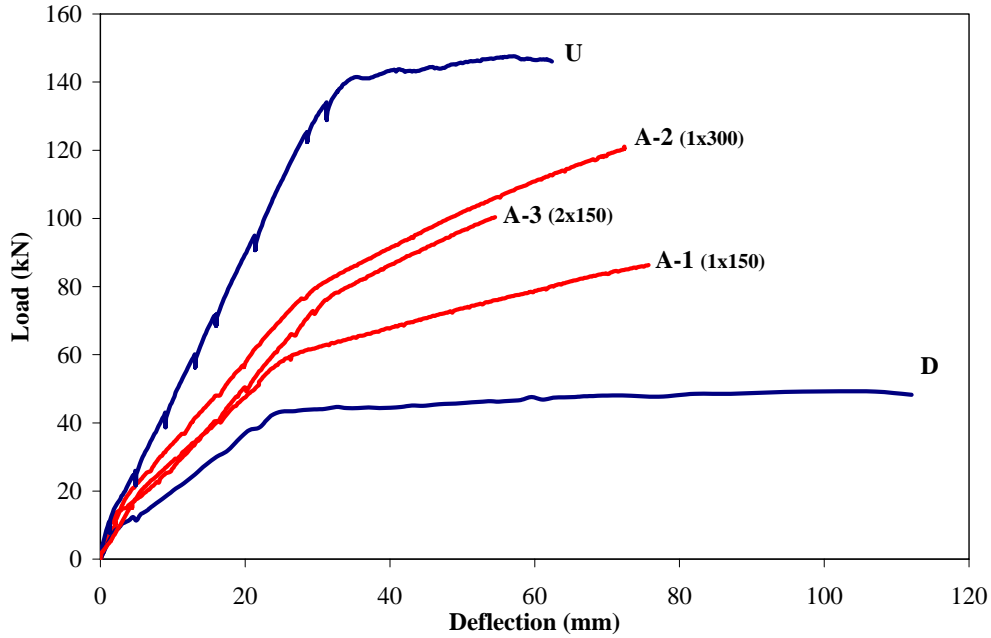


Figure 9 - Load-Deflection Curves: Control vs. 3X2 Bonded Beams

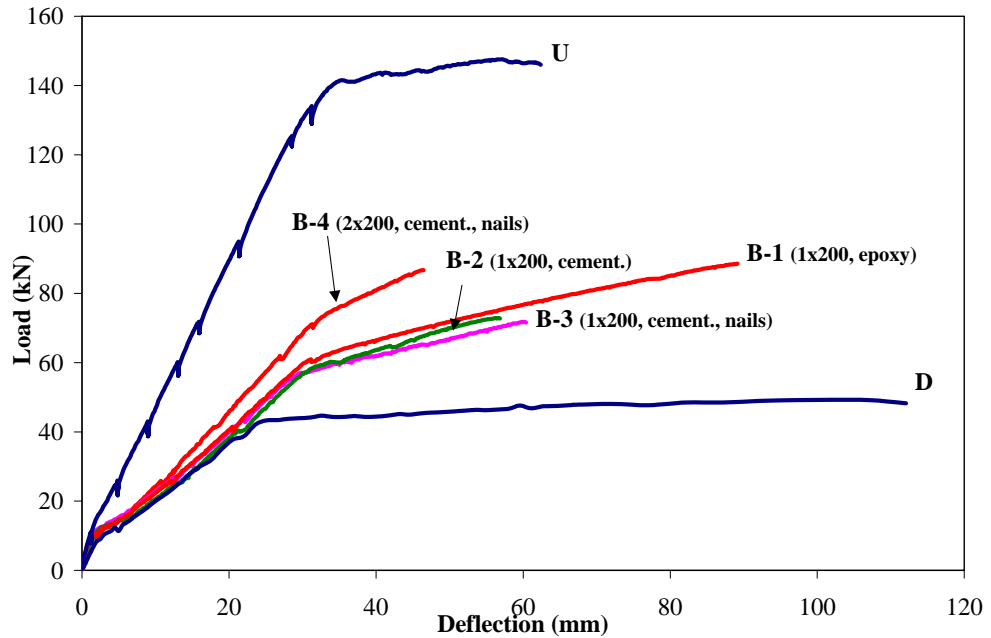


Figure 10 - Load-Deflection Curves: Control vs. 12X Bonded Beams

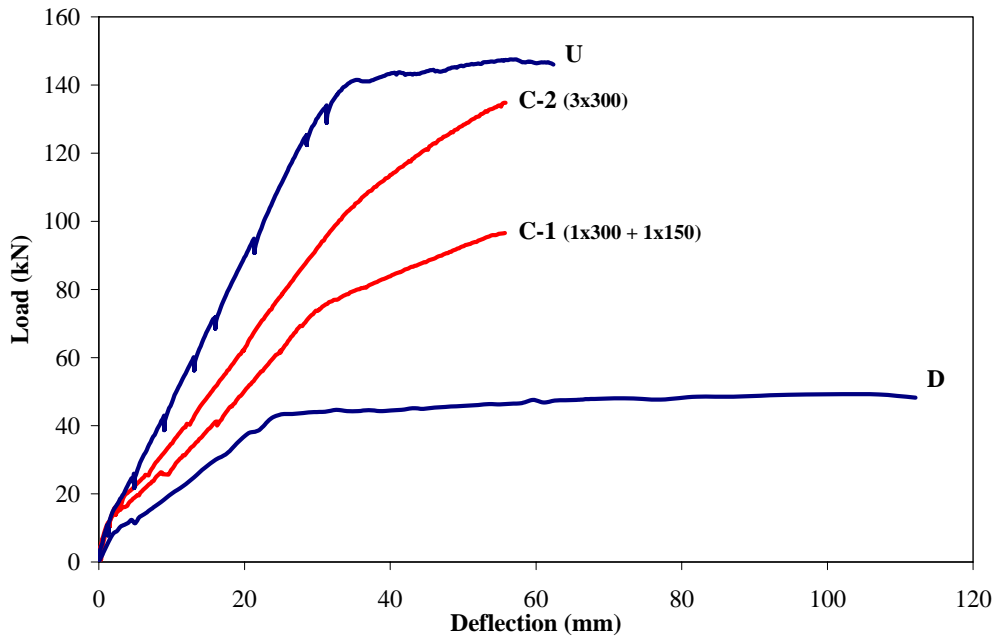


Figure 11 - Load-Deflection Curves: Control vs. FRP Bonded Beams

The installation of the 3x2 steel tape at the bottom of a Type D beam was beneficial in terms of first cracking (Figure 9). Regardless of width and number of plies, first cracking of Beams A-1, A-2 and A-3 occurred at a load of about 20 kN. A loss of stiffness is then observed; curves show a similar slope for Beams A-1 and A-3, which are less stiff than A-2. Then, further loss of stiffness is determined by yielding of the steel bars; A-1 yielded at 60.3 kN, while A-2 and A-3 reached the yielding at loads of 79.7 kN and 76.5 kN, respectively. After yielding the slope of each curve reflects the different amount of external reinforcement: A-2 and A-3, having the same amount of external steel tape, provide the same slope and are stiffer than A-1. The mode of failure was similar for the three beams: it was concrete cover separation (Figure 12 and Figure 13) which initiated at one of the loading points as described in literature (Teng et al. 2001). The minimum ultimate load within Group A beams was provided by A-1 whose failure occurred at about 86.3 kN; the maximum was attained by A-2 which failed at 121.1 kN. The tape layout based on the same area as for A-2, but arranged on two plies, limited the ultimate capacity of beam A-3 at 100.4 kN. This specimen exhibited the lower ultimate deflection (i.e., 54.5 mm); despite different ultimate strength, A-1 and A-2 showed similar ultimate deflections of 75.7 mm and 72.4 mm, respectively.



Figure 12 - Lateral View of Failure of A-2 Beam



Figure 13 - Bottom View of Failure of A-2 Beam



Figure 14 - Bottom View of Failure of B-1 Beam



Figure 15 - Bottom View of Failure of B-2 Beam

The installation of 12X steel tape did not affect significantly the first cracking of Group B beams (Figure 10), whose cracking loads were in the range of 9.2-11.5 kN. However, the corresponding deflections were reduced when compared to that of Beam D at same load (Table 11). The loss of stiffness due to cracking was very similar for beams B-1, B-2 and B-3; such similarity is also confirmed by very close values of yielding loads ranging between 57.1 and 60.4 kN (Table 11). Beam B-4, having twice the tape area, was stiffer than the other three and yielded at a load of 75.2 kN. The ultimate behavior highlights that Beams B-2 and B-3 failed at loads of 72.7 kN and 71.5 kN, respectively; this points out that the nails were unable to improve the ultimate performance of beam B-3, whose ultimate deflection (60.4 mm) was slightly larger than that of B-2 (56.8 mm). The epoxy resin allowed beam B-1, whose tape area was the same as for B-2 and B-3, to attain its failure at ultimate load and deflection equal to 88.6 kN and 89.2

mm, respectively. Similar strength performance was attained by beam B-4, whose failure occurred at 86.7 kN. Doubling the tape area enabled B-4 to reach an ultimate strength very close to that of an epoxy bonded beam with half the tape area (Beam B1), but reduced its ultimate deflection to 46.5 mm. The failure of Beams B-1 and B-2 was due to interfacial debonding which initiated at one of the loading points, as previously discussed in the literature (Teng et al. 2001). The epoxy allowed Beam B1 a better engagement of the concrete substrate than that provided by the cementitious grout on Beam B2; this can be observed by comparing Figure 14 and Figure 15. The failure of Beams B-3 and B-4 was also due to interfacial debonding after nail bearing failure (Figure 16).

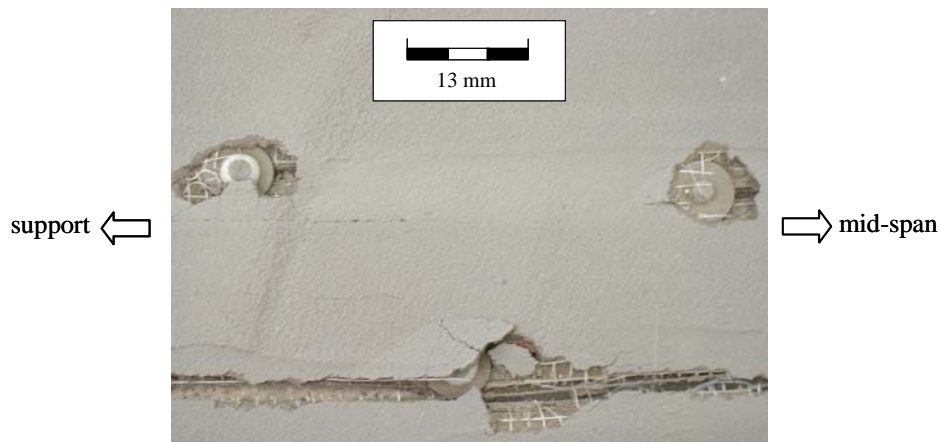


Figure 16 - Nail Bearing in Beam B-3

CFRP laminates increased cracking loads of Beams C-1 and C-2 (13.8 kN and 15.6 kN, respectively) when compared to reference Beam D (Figure 11). The loss of stiffness due to cracking was more significant for Beam C-1 than that of C-2, having twice the external FRP area. This determined also that its yield load (108.6 kN) was higher than that of C-1 (75.7 kN). After the yield point, curves of both specimens show further loss of stiffness that is again more significant for Beam C-1 than that of C-2. Both collapsed due to FRP debonding initiated at one of the loading points and characterized by separation of the concrete cover. Even though Beam C-2 failed at a load about 40% higher than C-1, their ultimate deflection was almost identical (55.8 mm vs. 55.7 mm).

Important information is also provided by the analysis of strain gage readings at both mid-span and termination of the externally bonded reinforcement of each beam. In this paper, the

discussion of local strains is limited to their average values. Average strains of the SRP tape in the constant moment region of Beams A-1 and A-2 were all close to 0.010, whereas an average value of 0.007 was recorded when two plies of 3X2 tape were used (Beam A-3). Beam B-1, whose 12X tape was bonded with epoxy, provided an average strain at mid-span equal to 0.012; the average strain recorded on the same tape bonded with cementitious mortar with and without nail anchors (Beams B-3 and B-2, respectively) was between 0.0051-0.006. A similar average value (0.005) was recorded when two plies of 12X tape was used (Beam B-4). Ultimate average strains at mid-span provided by beams strengthened with two plies (Beam C-1) and three plies (Beam C-2) of CFRP laminate were equal to 0.007 and 0.006, respectively.

Readings provided at beam failure by strain gages installed at the termination of the externally bonded reinforcement were less homogeneous than those obtained at mid-span due to the well-known effect of stress concentration at the termination of the plates (Cosenza and Pecce 2001). In general, at the end of beams bonded with the 3X2 tape (Type A beams) average ultimate strains were in the order of 0.0001 with peak values up to 0.0005. Average strains in the order of 0.00007 were recorded at the end of 12X tapes (Type B beams) with peaks up to 0.0003. Average strains in the order of 0.0002 were given by CFRP laminates with peak values up to 0.002.

5.7 Discussion

The analysis of the test results is conducted first with respect to beams strengthened with the same external reinforcement (3X2 tape, 12X tape and CFRP laminate); then, beams characterized by similar $\bar{\epsilon}_{eq}$ achieved with different materials are compared. Remarks on the influence of different reinforcement type and layout on crack widths are also presented.

For each group of beams strengthened with the same system, the following can be highlighted:

- Up to the yielding of the internal steel reinforcing bars, the slope of the load-deflection curve of Beam A-3 is very similar to that of A-1, that had an external tape area of only half of that in A-3. A-2, equivalent to A-3 in terms of tape area, exhibited a stiffer behavior prior to steel yielding. This is also evidenced by the fact that average crack widths were almost identical for Beams A-1 and A-3, but were wider than those exhibited by Beam A-2. Considering that crack spacing was similar for all tested beams and equal

approximately to about the stirrup spacing (100 mm), outcomes provided by Group A beams suggest that the capability of the externally bonded SRP to reduce crack width and to stiffen the member in the pre-yielding phase is strongly dependent on the width of the external reinforcement rather than on its sectional area (Ceroni et al. 2004);

- By doubling the width of the 3X2 steel tape the ultimate strength increased by about 40% (A-2 vs. A-1), while the ultimate deflection was quite similar. When the same area increase was achieved by doubling the number of plies rather than width (Beam A-3), the strength increased only by about 16% compared to Beam A-1 due to a high concentration of interfacial stresses; the ultimate deflection was about 28% lower due to a lower stiffening effect already observed in the pre-yielding field. Overall, if compared to beam D the 3X2 steel tape provided increases of the ultimate strength ranging between 75% (A-1) and 145% (A-2), even though the ultimate deflection had reductions ranging between 25% (A-1) and 46% (A-3);
- No significant stiffening was provided by the 12X steel tape installed on Beams B-1, B-2 and B-3 with epoxy and cementitious grout in the pre-yielding field; the load-deflection behavior of Beam B-4 appeared slightly stiffer than Beam D after a load of about 25 kN. Such result suggests that the structure of the 12X tape makes it less stiff than 3X2 and its effectiveness in reducing crack width (Ceroni et al. 2004) and stiffening the flexural element is negligible;
- The epoxy resin impregnation made Beam B-1 able to withstand ultimate load and deflection about 23% and 53% larger than those seen in equivalent Beams B-2 and B-3 bonded with cementitious grout, respectively. In order to attain with cementitious grout the strength provided by epoxy resin, it was necessary to double the area of 12X tape (Beam B-1 vs. B-4); however, the ultimate deflection of Beam B-4 was 48% smaller than that of B-1. The use of nail anchors to improve the bond of the 12X tape was not effective in terms of strength, even though the ultimate deflection of Beam B-3 was about 6.5% larger than that of B-2. If compared to beam D, schemes based on 12X tape determined strength increase ranging between 46% (B-3) and 79% (B-1), with reductions of ultimate deflection ranging between 13% (B-1) and 55% (B-4).

- The installation of CFRP affected the stiffness of strengthened beams and this was confirmed also by crack width trends (Ceroni et al. 2004). By doubling the area of CFRP, the ultimate strength of Beam C-2 was about 39% higher than that of C-1; the ultimate deflections were almost identical. If compared to Beam D, the CFRP reinforcement allowed boosting the strength by percentages ranging between 95% and 173%; a reduction of ultimate deflections of 45% was measured for both C-1 and C-2.

The effectiveness of different strengthening solutions can be assessed by comparing flexural members with similar ρ_{eq} and considering that:

- Slopes of load-deflection curves of Beams A-1, B-1, B-2, B-3 and C-1, characterized by ρ_{eq} ranging between 0.65 and 0.69, are very similar up to yielding of the tensile bars. Tape 3X2 impregnated with epoxy (A-1) was more effective in delaying the first cracking compared with the CFRP laminate (C-1). Tape 12X impregnated with epoxy (beam B-1) or with cementitious (B-2 and B-3) did not increase the cracking load of the unstrengthened Beam D. Load-deflection branches between first cracking and steel yielding of Beams A-1 and C-1 are almost identical; a comparison highlights that both were stiffer than B-1, B-2 and B-3. It was also observed that Beams A-1 and C-1 provided almost equal average crack widths and were more capable to reduce crack widths than the other three equivalent Beams (Ceroni et al. 2004). The yielding of the steel bars for Beams A-1, B-1, B-2 and B-3 occurred at similar loads and deflections (Table 11). The yielding load of Beam C-1 was higher by about 29% and corresponded to a similar deflection. Branches of load-deflection curves after steel yielding are approximately parallel, except for Beam C-1 that was stiffer. If impregnated with epoxy, the 12X tape allowed Beam B-1 to attain a ultimate deflection about 18% larger than A-1 even though both provided the same strength; when it was impregnated with cementitious grout (Beam B-2) or eventually nailed (Beam B-3) such tape provided ultimate strength and deflection about 16% and 23% smaller than those attained by beam A-1. The stiffness of the CFRP laminate higher than that of the SRP laminate (resulting in a post-yield slope of C-1 steeper than that for A-1 as depicted in Figure 9 and Figure 11)

allowed Beam C-1 to attain an ultimate strength about 12% larger than A-1, even though its ultimate deflection was 26% smaller;

- By comparing the slopes of load-deflection curves of Beams A-2, A-3, B-4 and C-2 (characterized by ρ_{eq} ranging between 0.72 and 0.79) it is observed that Tape 3X2 impregnated with epoxy (A-2 and A-3) was very effective in delaying the first cracking; the CFRP reinforcement had some influence on cracking initiation (C-2), which was not affected by the installation of tape 12X impregnated with cementitious and anchored with nails (B-4) (Table 11). Slopes of branches between first cracking and steel yielding highlight a stiffening effect which was maximum for Beams A-2 and C-2, decreased for Beam A-3 and was not observed in the case of Beam B-4. Such trend was confirmed also by a comparison in terms of capacity of the externally bonded system to reduce crack widths (Ceroni et al. 2004). Yielding of steel bars for Beams A-2, A-3 and B-4 occurred at similar loads and deflections (Table 11). The yielding of Beam C-2 occurred at load and deflection about 41% and 15% higher, respectively. Branches of load-deflection curves after steel yielding are about parallel for Beams A-2, A-3 and B-4; Beam C-2 provides a stiffer trend that could be partially due to the slight difference of ρ_{eq} with others (Table 11). The lower bond performance of the cementitious grout affected the strength of Beam B-4 which was 71% and 86% that of Beams A-2 and A-3 bonded with epoxy resin, respectively. Its ultimate deflection was 65% and 85% that of A-2 and A-3, respectively. The influence of stress concentration that limited the ultimate performance of A-3 (two plies) if compared to A-2 (one ply) was already discussed. Beam C-2 provided a strength 11% higher than A-2 with a ultimate deflection 23% smaller. Beams A-2 and C-2 exhibited ultimate strength in the order of 82% and 91% that of Beam U even though their ρ_{eq} was about equal to 49% and 52% that of Beam U, respectively. These data have particular relevance if one considers that for both A-2 and C-2 the full capacity of the cross-section was not exploited due to debonding of the externally bonded reinforcement. In terms of ultimate deflections, Beams A-2 and C-2 attained values equal to 1.26 and 0.98 times that provided by beam U, respectively (Table 11).

5.8 Conclusions

The laboratory investigation presents an experimental study aimed at assessing the potential of SRP to provide a strengthening system alternative to traditional techniques and to FRP laminates. SRP-based solutions utilize improved traditional materials (steel and cementitious grout). This could be advantageous over FRP and overcome its problem areas such as high cost of constituents (fibers and epoxy matrix), fire resistance, low confidence and experience with non-traditional materials, and incompatibility with mechanical anchorages due to stress concentration.

Experimental tests were conducted in order to assess the structural effectiveness of SRP and evaluate the influence of epoxy versus cementitious matrix; the possibility of using nail anchors to improve the bond of steel tapes impregnated with cementitious grout was also verified. The performance of seven SRP reinforced beams were compared to that of unstrengthened and FRP reinforced beams. This preliminary analysis of test results underlined that:

- Strength increases provided by SRP bonded with cementitious grout were smaller than those obtained using epoxy. CFRP was more effective than epoxy bonded SRP in terms of strength; the trend was inverted in terms of ultimate deflections. Compared to the unstrengthened beam, SRP allowed attaining strength increases ranging between 46% and 145%, while reductions of ultimate deflections ranged between 13% and 55%. A comparison between beams with equivalent reinforcement ratio highlights that epoxy bonded SRP tapes provided ultimate strength about 10% smaller than CFRP with deflections about 24% larger.
- The epoxy resin was more effective than the cementitious grout in engaging the concrete substrate; regardless of the type of matrix (epoxy or cementitious), the behavior of equivalent (same area of external reinforcement) SRP strengthened beams was similar up to yielding of the internal steel. At ultimate, the epoxy SRP ultimate strength and mid-span deflection were about 23% and 53% larger than those corresponding to the SRP impregnated with cementitious grout.
- The nail anchors did not improve the performance of the SRP impregnated with cementitious grout. The lack of transverse link in the steel tape did not allow distributing

the local stress concentration at anchor location; this determined the local bearing failure of nails that were unable to improve the bond and delay tape debonding.

- The 3X2 tape affected the global stiffness of strengthened beams and this effect was dependent on the width rather than on the area of the bonded tape. The different macrostructure made the 12X tape unable to provide any stiffening effect. Such trends were confirmed by recorded widths of cracks, whose spacing was very similar for all tested beams.
- Strains recorded at failure on the externally bonded reinforcement in the constant moment region indicated that interfacial issues and their influence on failure modes are mainly dependent on the matrix (i.e., epoxy versus cementitious) rather than on the type of fiber (steel versus carbon). Strain values were consistent when epoxy was used to bond the 3X2 tape (Type A beams), the 12X tape (Beam B-1) and CFRP (Type C beams); average values of about 0.010, 0.007 and 0.006 were found for one, two and three plies, respectively. When the SRP was bonded with the cementitious mortar (Beams B-2, B-3 and B-4), those values were in the order of 0.006 and 0.005 for one and two plies, respectively. These trends confirm that when the cementitious mortar was used the debonding occurred earlier compared with the epoxy resin as it was highlighted by the different engagement on the concrete substrate after failure. These data will provide an important background for the extension of design criteria developed for FRP laminates to the case of SRP tapes bonded with either epoxy resin or cementitious mortar.
- Laboratory outcomes confirmed the effectiveness of SRP for the flexural strengthening of RC members. Even though smaller than CFRP, strength increases provided by SRP were significant if compared to upper limits that the strengthening design needs to respect in compliance with ACI 440 (2002) guidelines. Epoxy bonded SRP performed better than FRP in terms of ultimate deflection; this could be very important especially for structures that require a high displacement capacity. Overall, SRP strengthening systems appeared to be a promising technique that could be alternative to FRP when durability is not a critical requirement, even though more research is needed on this aspect. The system could be further optimized by improving the bond of the cementitious grout and by

developing effective mechanical anchorages able to prevent or delay delamination. The experimental results presented in the paper could represent a first step for the development of code recommendations for the design of flexural strengthening of RC structures using SRP.

6 FIELD TESTING

6.1 Introduction

The opportunity for experimenting this new material in the field, became available in the winter of 2003 when the City of Bloomington, Indiana, decommissioned an existing parking garage near the downtown area, built with double-T PC beams. The concrete repair contractor, Structural Preservation Systems, Hanover, MD, strengthened in flexure the bottom stem of several double-T beams with epoxy-based SRP. In the followings are reported the experimental as well as analytical results of tests to failure conducted on three beams: a control specimen, a beam strengthened with one ply of SRP and a third beam strengthened with two plies of SRP anchored at both ends with U-wraps.

6.2 Experimental Program

6.2.1 Building Characteristics

The parking garage used for the tests was a two storey structure constructed in the 1980s (see Figure 17). It consisted of a reinforced concrete (RC) frame, cast in place columns and precast reversed-T PC beams, supporting double-T PC beams, of span length varying from 4.66 m (15.3 ft) to 13.41 m (44 ft).



a) Side View of Parking Garage



b) Top View of the Deck



c) Bottom View of the Deck

Figure 17– Bloomington Parking Garage

Since no maintenance or construction records were available for the materials and the layout of the prestressing tendons, a field investigation was carried out. Based on the survey, it was determined that the double-T PC beams were of type 8DT32 according to the Prestressed Concrete Institute (1999) specifications (see Figure 18) with concrete topping of 76 mm (3 in), and with an arrangement of the tendons different from current specifications.

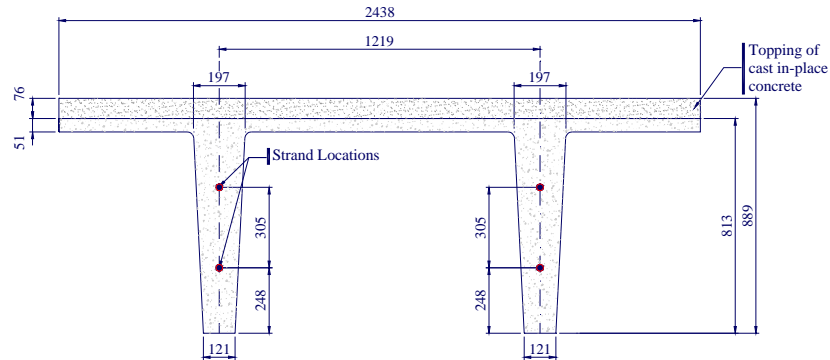


Figure 18 – Double-T Geometry Details (*SI units 1 mm = 0.039 in*)

For the span of 4.66 m (15.3 ft), two straight 7-wire strands were found in each stem, each with a diameter of 12.7 mm (0.5 in), corresponding to an area of 112 mm² (0.174 in²), the first at 248 mm (9.75 in) from the bottom of the stem and the second spaced 305 mm (1 ft) from the first one (see Figure 18). No mild reinforcement was found at any location. Welded pockets, connecting two adjacent beams, were positioned every 910 mm (3 ft) at a depth of 76 mm (3 in) from top surface. Concrete properties were evaluated using three cores taken from three different beams at the location of the stem and an average concrete cylinder strength of $f_c' = 34 \text{ N/mm}^2$ ($f_c' = 5000 \text{ psi}$) was found and its module of elasticity was determined according to ACI 318-02 Section 8.5.1 provisions (see Table 15). The strands properties were assumed to be conventional 1861 MPa (270 ksi) strength and summarized in Table 15.

Table 15 - Properties of Construction Materials

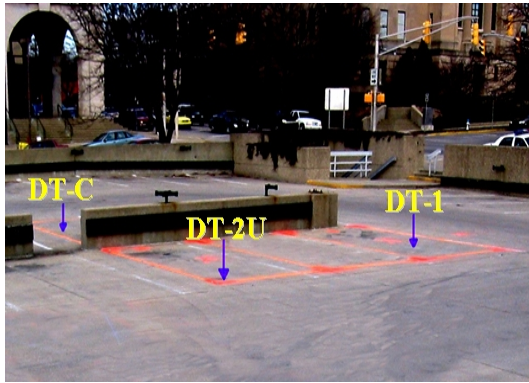
Material	Cylinder Compressive Strength, MPa (psi)	Yield Strength MPa (ksi)	Rupture Strength MPa (ksi)	Elastic modulus ⁽²⁾ MPa (ksi)	7 wire Tendon Cross Section, Ap mm ² (in ²)
Concrete ⁽¹⁾	34.4 (5,000)	-	-	27,600 (4,000)	-
Steel	-	1585 (230)	1862 (270)	200,000 (29,000)	112 (0.174)

⁽¹⁾ Average of 3 specimens [76.2 mm×152.4 mm (3 in×6 in) cylinders].

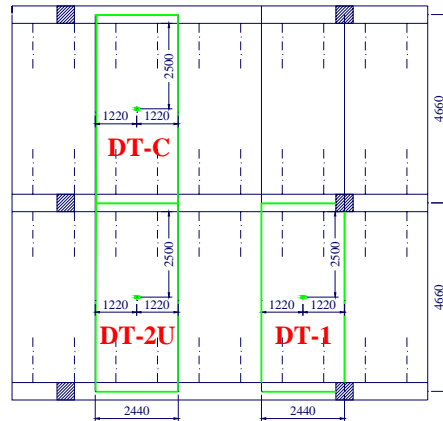
⁽²⁾ $E_c = 4700 \sqrt{f_c'}$ ACI 318 Section 8.5.1

6.2.2 Specimens and Installation of Steel Reinforced Polymer

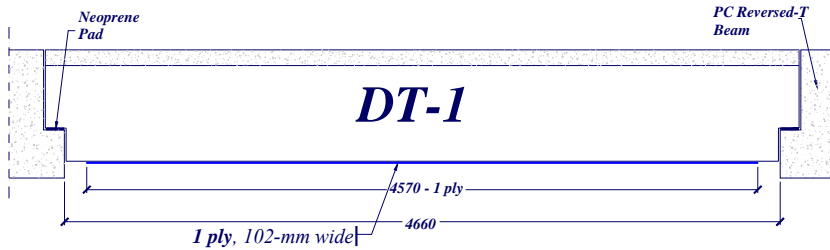
A total of three double-T PC beams were tested (see Figure 19): beam DT-C is the control beam, beam DT-1 represents the beam strengthened with one ply of SRP and DT-2U the one strengthened with 2 plies of SRP anchored with SRP U-wraps.



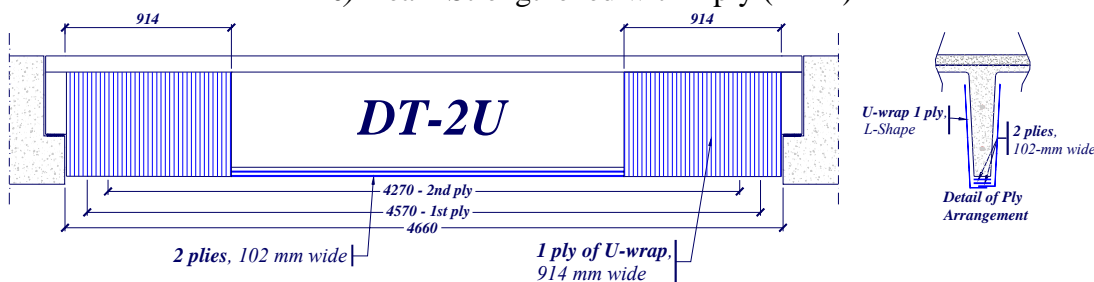
a) Saw-Cut Marks on Top of Deck



b) Plan View



c) Beam Strengthened with 1 ply (DT-1)



d) Beam Strengthened with 2 plies + U-wrap (DT-2U)

Figure 19 – Test Beams (SI units 1 mm = 0.039 in)

The epoxy resin for both strengthened beams was SikaDur Resin 330 (Sika 2005). Table 16 reports the resin properties supplied by the manufacturer and verified by testing according to ASTM D 3039 standards during the characterization laboratory work. The choice of the resin was based on constructability so that it could be rolled onto the surface for overhead applications, while having enough consistency, even before curing, to be able to hold the weight of the steel tape during cure.

Table 16 - Mechanical Properties of Epoxy Resin

Matrix	Tensile Strength, MPa (psi)	Ultimate Rupture Strain ϵ_{fu}^* (mm/mm)	Tensile Modulus of Elasticity, MPa (ksi)
SikaDur 330 ⁽¹⁾	30 (4350)	1.5	3800 (551)

⁽¹⁾Values provided by the manufacturer (Sika, 2002)

The tape was medium density consisting of 6.3 cords per cm (12 WPI), with material properties defined in Table 17.

Table 17 - Material Properties of Steel Tape

Cord Coating	Cord Area per 12 Wires, mm ² (in ²)	Cords per cm (in)	Nominal Thickness ⁽¹⁾ , t _{SRP} mm (in)	Tensile Strength f _{fu_SRP} , MPa (ksi)	Ultimate Rupture Strain ϵ_{fu_SRP} (mm/mm)	Tensile Modulus of Elasticity, GPa (ksi)
Brass	0.396 (0.000615)	3.7 (9.5)	0.148 (0.0058)	3070 (447)	0.0167	184 (26700)

⁽¹⁾ The nominal thickness has been computed assuming the area of each cord and counting the number of cords in each ply, reported in *cords per cm*

The typical stress-strain diagram for an impregnated medium density tape, tested following the ASTM D 3039 recommendations, is reported in Figure 20 (properties based on steel net area).

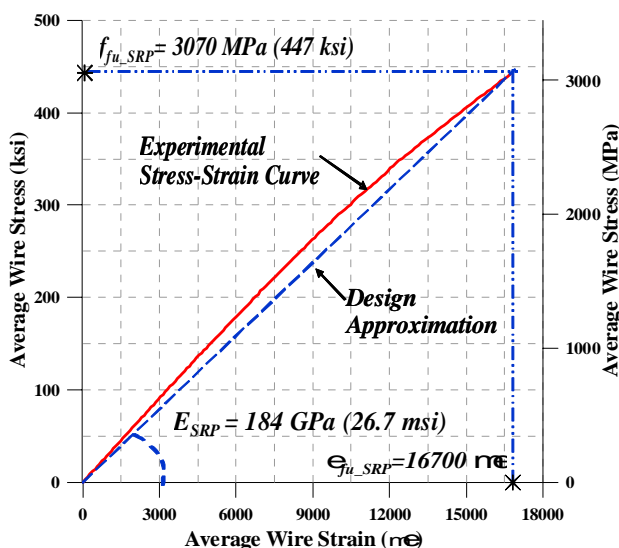


Figure 20 – SRP Laminate Stress vs Strain Behavior

SRP was installed following the recommendations of ACI 440.2R-02 (ACI 440) provisions for FRP materials. The sequence of installation steps is reported in Figure 21. The bottom stem of

the double-T beams was first abrasive-blasted to ensure proper bond of the SRP system. With the surface roughened and cleaned, the first layer of epoxy was directly applied (see Figure 21b), without primer coating. The steel tape was cut to length of 4.57 m (15 ft) and width of 102 mm (4 in), covering the bottom of the stem length and width entirely. A rib-roller was then utilized to press onto the tape to ensure epoxy impregnation and encapsulation of each cord and allow excess resin to squeeze out. The excess resin was spread with a putty-knife to create an even surface (see Figure 21c) and a synthetic scrim was applied to avoid any dripping of the resin (see Figure 21d). For the two ply application, once the first ply was in place and the excess resin leveled, the second ply was installed, following an identical procedure. This time the ply started 152 mm (6 in) away from the terminations of the first ply, making it 4.27 m (14 ft) long. To provide a mechanical anchorage for the two longitudinal plies, an SRP U-wrap 914 mm (3 ft) wide was installed at both ends of the stems (see Figure 21e). Due to the stiffness of the steel tape, pre-forming is done with a standard sheet metal bender before installation. For this reason, the U-wrap was obtained by overlapping two L-shaped wraps.

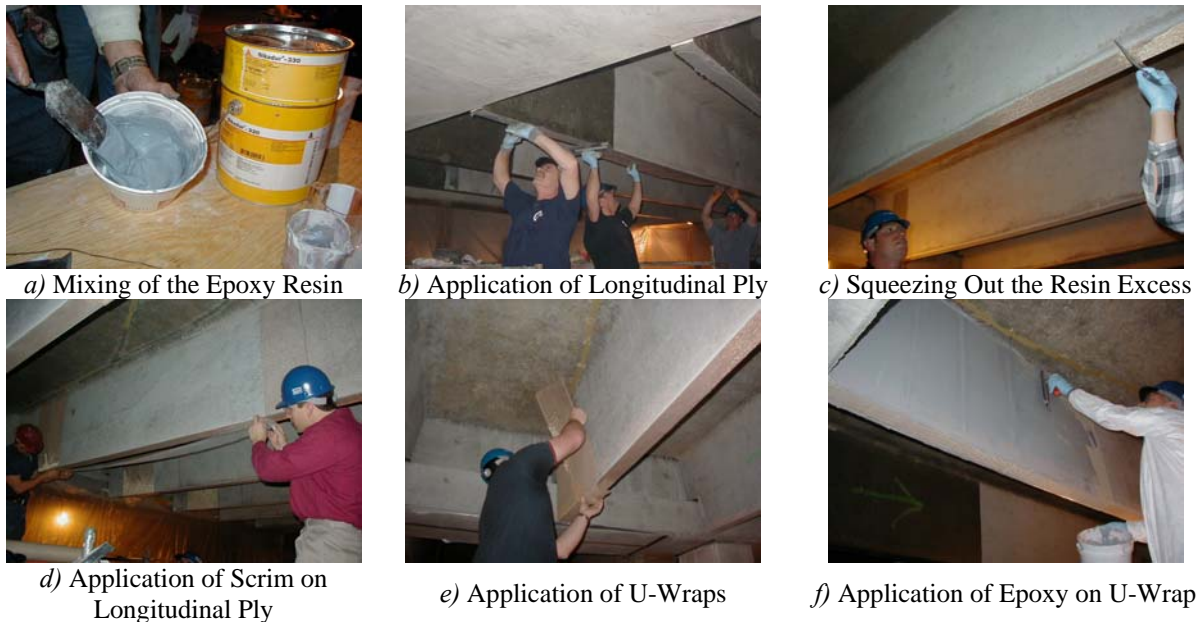


Figure 21 – SRP Installation Procedure

6.2.3 Test Setup and Instrumentation

The experimental setup is shown in Figure 22a and Figure 22b. The beams were tested under simply supported conditions and subject to a single concentrated load spread over both stems at mid-span, that is, 3-point bending at mid-span (see Figure 22c).

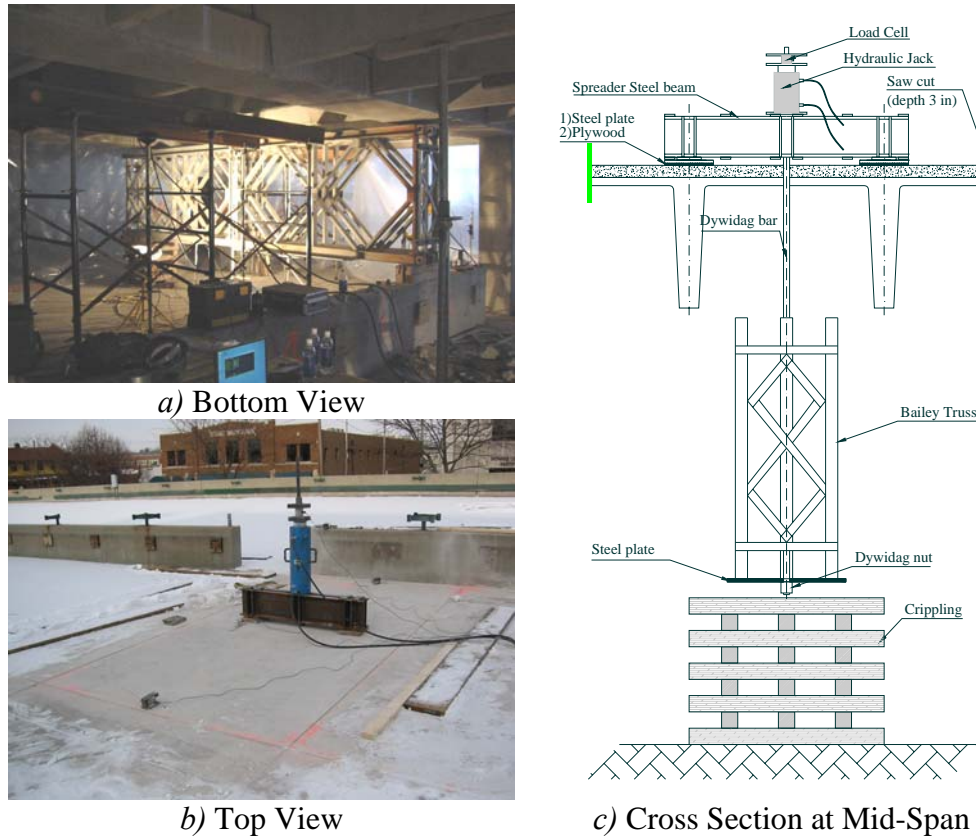


Figure 22 – Test Set Up

All three tests were conducted using a close-loop load configuration, where no external reaction is required. The load was applied in cycles by one hydraulic jack of 890 kN (200 kip) capacity connected to a hand-pump. The load was transferred to the PC beam in two points through one spreader steel beam (see Figure 22b). The reverse-T PC-Ledger beams, on which the double-T beam rests, supplied the reaction. As the hydraulic jack extended, it pulled on the high-strength steel bars, which lifted the reaction bailey-truss below. The reaction truss was built with three bailey-truss frames 6.09 m (20 ft) long assembled as per manufacturer’s specifications (Mabey Bridge and Shore, Baltimore, MD), and properly designed to carry the test load (see Figure 22a). Plywood was placed at each contact point to protect the concrete. The load was measured using a 890 kN (200 kip) load cell placed on top of the jack (see Figure 22c). The preparation work consisted of drilling one hole of small diameter (~50 mm (2 in)) necessary for passing the high-strength steel bar through the flange of the double-T PC beam and isolating each test specimen from the adjacent beams originally joined by the welded-pockets.

An electronic data acquisition system (see Figure 23a) recorded data from four linear variable differential transducers (LVDTs) and two electrical strain-gages applied to the SRP in beams DT-1 and DT-2U. Two LVDTs were placed at mid-span (see Figure 23b), and the remaining two LVDTs, were placed under the reverse-T ledger beams to verify potential support settlements. Strain gages were installed at mid-span on the bottom flange of the two strengthened double-T beams, directly onto the SRP material.

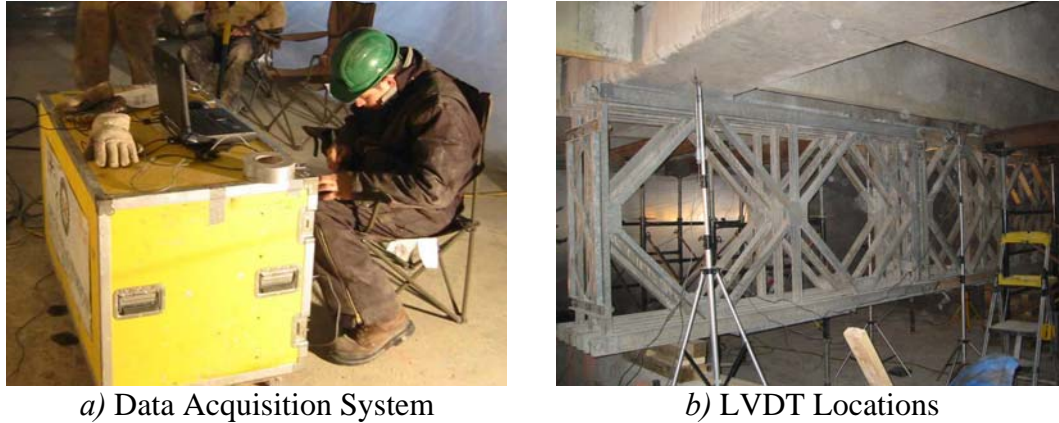


Figure 23 – Installed Instrumentation

6.2.4 On-Site Safety

Safety procedures were adopted during the performance of the tests. The parking garage areas affected by each test were fenced and no one allowed within such areas. Shoring was provided and designed to carry the weight of the beam tested (multiplied by a safety factor equal to 2.0 to account for impact) and the additional weight of the testing equipment. Shoring was not in direct contact with the beam stems to allow unobstructed deflection.

Table 18 - Beam Test Results

Beam	Failure load kN (kip)	Load Capacity Increase	SRP Strain at Failure ϵ_{SRP} (‰)	Failure Mode
DT-C	344 (77.4)	1	-	Rupture of Lower Tendon
DT-1	387 (87)	1.12	12280	SRP Delamination
DT-2U	434 (97.6)	1.26	6400	Rupture of Lower Tendon

6.3 Results and Discussion

All beams failed in flexure and had a similar behavior up to the cracking load. Beam DT-C failed due to fracture of the lowest tendon. In beam DT-1, since the SRP ply was not mechanically anchored, failure was dictated by peel off of the ply from each stem almost

simultaneously. Beam DT-2U, strengthened with two anchored plies per stem, failed due to rupture of the lower tendon. Table 18 reports the test results.

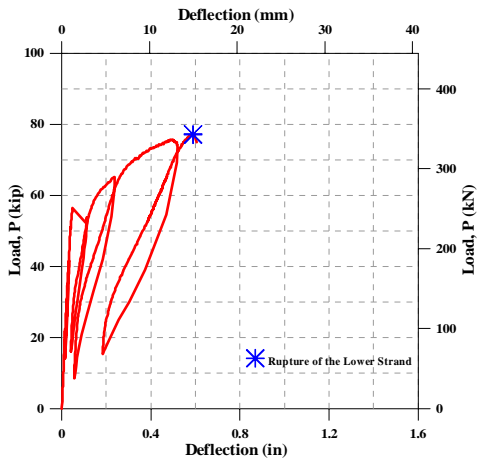


Figure 24 – Load vs Mid-Span Deflection
(Beam DT-C)

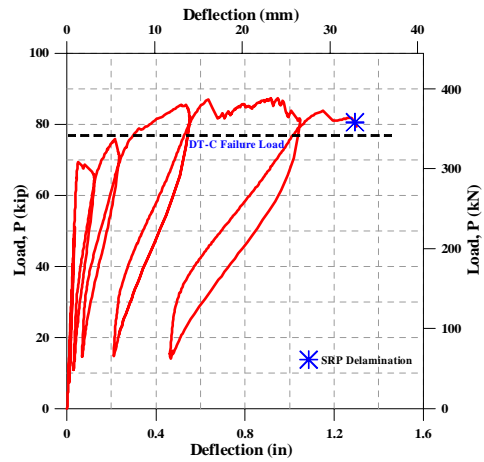


Figure 25 – Load vs Mid-Span Deflection
(Beam DT-1)

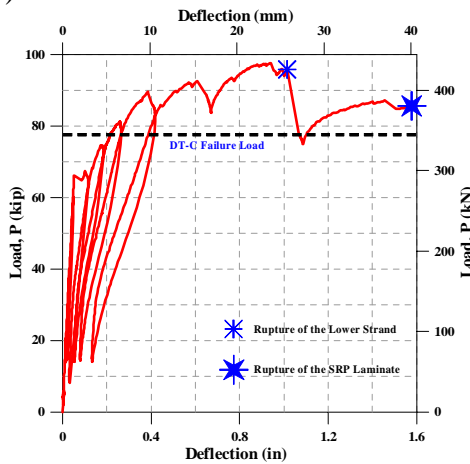


Figure 26 – Load vs Mid-Span Deflection (Beam DT-2U)

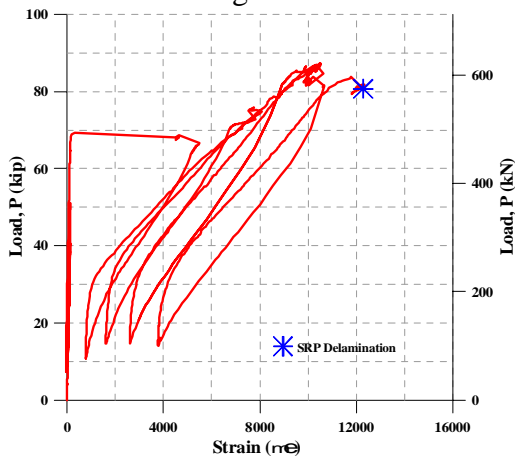


Figure 27 – Load vs Mid-Span Strain (Beam DT-1)

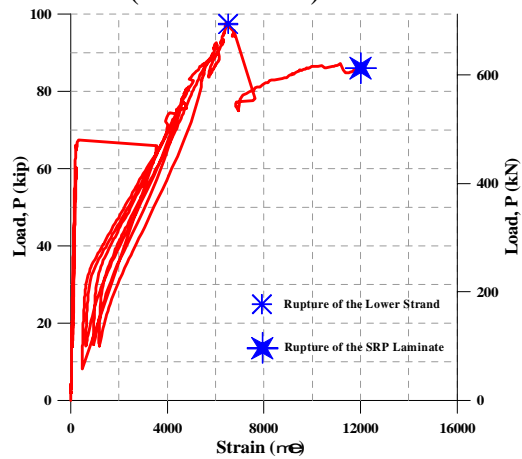
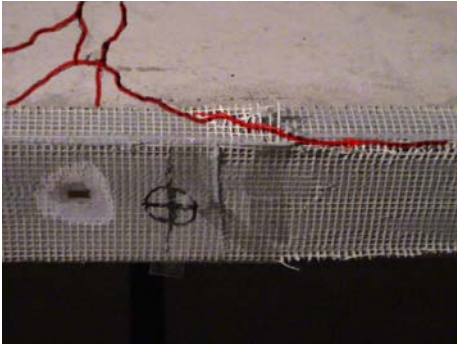
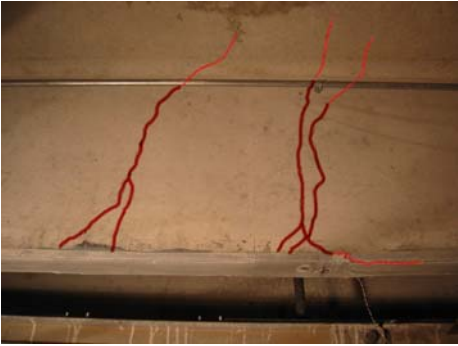


Figure 28 – Load vs Mid-Span Strain (Beam DT-2U)

In beam DT-C flexural cracks were concentrated in the mid-span region where the point load was applied. As soon as cracking occurred, since no mild reinforcement was present and tendons were placed far away from the bottom of the stem, cracks developed throughout the entire stem. In beams DT-1 and DT-2U a similar behavior occurred with the difference that the presence of the SRP allowed the formation of additional flexural cracks (see Figure 29). In beam DT-1 the SRP laminate started debonding at mid-span initiated by the widening of mid-span cracks (see Figure 29a) and then progressed towards the supports (see Figure 29b). Complete detachment of the laminate occurred at one end of the beam with part of the concrete substrate attached to the laminate, denoting a good interface bond between the concrete and the SRP. In beam DT-2, SRP could not completely peel off due to the presence of U-wraps. Delamination propagated from mid-span towards the supports similarly to Beam DT-1, until rupture of the lower tendon occurred and immediately followed by SRP rupture exactly at the location where the SRP U-wrap started. No shear cracks were noted on any of the three beams.



a) Crack Propagation Prior to Complete Peeling b) Debonding Propagation from Mid-Span
Beam DT-1



c) SRP Rupture d) Rupture of the Lower Tendon
Beam DT-2U

Figure 29 – Failure Mechanisms in Strengthened Beams

Figure 24 through Figure 26 shows the Load-vs-mid-span Deflection curves for all three beams. The capacities of beams DT-1 and DT-2U increased approximately 12 and 26% with respect to the control specimen DT-C.

Figure 27 and Figure 28 report the Load-vs-Mid-Span Strain responses for beams DT-1 and DT-2U. Two distinct phases, pre- and post-cracking, characterize the behavior of each specimen. Up to cracking there was practically no strain in the SRP. Past the cracking load, the presence of the SRP significantly affected performance.

Beam DT-C (see Figure 24) cracked at a considerably lower load (250.8 kN (56.4 kip)), with respect to the other two strengthened specimens. The occurrence of the first crack, at mid-span only, corresponds to the load drop in the Load-vs-Displacement plot. Upon unloading, the beam remained almost perfectly elastic, recovering almost all deflection. At the third loading cycle the lower strand suddenly fractured at a load of 344.3 kN (77.4 kip).

For beams DT-1 and DT-2U the cracking load increased of approximately 23% and 17% with respect to DT-C (see Figure 25 and Figure 26). The lower cracking load for DT-2U may be explained by the fact that the beam had been previously repaired by means of epoxy injection.

Beam DT-1 reached the peak load of 387 kN (87 kip) and held it constant with increasing deflection, while SRP progressively delaminated from mid-span towards the support. The strain profile reported in Figure 27 shows how the SRP was not engaged until cracking occurred and as soon as the first crack opened at mid-span, the SRP bridged the crack and strain suddenly increased to approximately 5500 $\mu\epsilon$ (strain-gauge was placed at mid span where the first crack occurred). The maximum strain recorded in the steel tape (12300 $\mu\epsilon$), prior to complete peel-off, shows how the material was well bonded to the concrete substrate. The ductility reported in the load-deflection curve, is the result of the slow peeling propagation rather than to the yielding of the reinforcing steel tape itself. Figure 25 shows in fact an almost elastic behavior till rupture of the SRP laminate.

Past the cracking load (Figure 26), beam DT-2U behaved almost linearly, although with a lower stiffness, until it reached the load of 400 kN (90 kip) then, stiffness decreased significantly till the peak load was reached. When the load of 434 kN (97.6 kip) was reached, the lower tendon ruptured and a sudden drop in the load-deflection curve was recorded. The strain in the SRP material at time which the tendon ruptured was 6400 $\mu\epsilon$. At this stage, once the lower tendon

ruptured, the SRP laminate was completely debonded except for the region where anchoring was provided by the U-wraps. The test was continued until suddenly the SRP laminate ruptured at 388 kN (87.2 kip). The strain recorded in the SRP laminate at failure was 12000 $\mu\epsilon$, similarly the values attained in beam DT-1.

6.4 Analytical approach

The conventional analytical approach outlined in ACI 318-02 (2002) was used in conjunction with ACI 440 provisions to compute the ultimate capacity of the beams without considering safety factors normally included in design.

The SRP behavior was approximated as illustrated in Figure 20 and the values used for f_{fu_SRP} , e_{fu_SRP} , and E_{SRP} are reported in Table 17.

The moment capacity M_n , inclusive of the SRP strengthening, can then be computed following ACI 440 provisions, using the appropriate equations to compute α and β_1 (Todeschini et al. 1998) so that a rectangular stress block suitable for the particular level of strain in the concrete could be used, as (see also Figure 30):

$$M_{n_SRP} = A_{pB} f_{pB} \left(d_{pB} - \frac{\beta_1 c}{2} \right) + A_{pT} f_{pT} \left(d_{pT} - \frac{\beta_1 c}{2} \right) + A_{SRP} f_{fe_SRP} \left(h - \frac{\beta_1 c}{2} \right) \quad (11)$$

where the first two terms of the equation represent the existing prestress steel reinforcement, with the index pB and pT indicating the contribution of the bottom and top tendons, and assuming the following:

- total losses in the prestress tendons : 30%
- in-place moment, prior to testing, only due to beam self weight .

The third term, of Eq.(11), represents the SRP contribution with the following assumptions being made:

- the area of SRP is computed as:

$$A_{SRP} = n(t_{SRP} \cdot w_{SRP}) \quad (12)$$

where the n represents the number of plies, t_{SRP} the thickness of one ply (obtained by multiplying the area of one cord per the number of cords in the installed ply and dividing by the width of the ply) and w_{SRP} the width of the ply;

- the k_m , bond reduction factor used to compute the effective stress in the SRP, has been computed according to ACI 440 provisions, using SI units, as follow:

$$\kappa_m = \frac{1}{60\varepsilon_{fu_SRP}} \cdot \left(1 - \frac{nE_{SRP}t_{SRP}}{360,000} \right) \leq 0.90 \quad (13)$$

being $nE_{SRP}t_{SRP} \leq 180,000$ for both beams DT-1 and DT-2U.

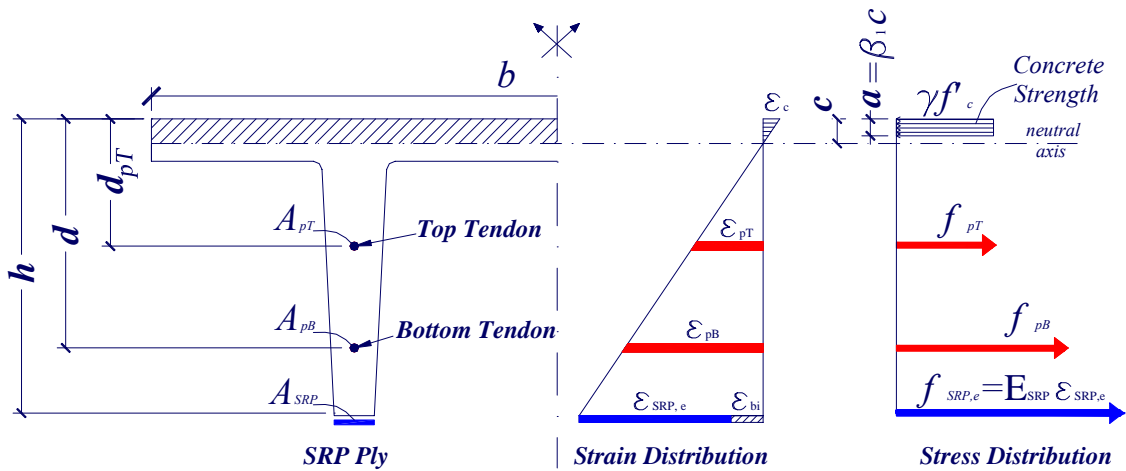


Figure 30 – Strain and Stress Distribution Across Beam Depth

Table 19 reports on the analytical results. As reported in the second column, none of the tested beams reached the ultimate compression strain of $\varepsilon_{cu}:0.003$. Beam DT-C was found to fail in tension due to rupture of the lower tendon, as found experimentally, with a strain in the lower tendon of $\varepsilon_{pB}:0.023$ and the ultimate failure load was found to be less than the experimental by only 2%. Both Beam DT-1 and DT-2U were found to fail due to attainment of the effective SRP strain value, that were 0.0149 and 0.0139 for beams DT-1 and DT-2U respectively. Even though the experimental and analytical capacity values are very close, a convincing and exhaustive calibration of the k_m factor and the corresponding delamination need to be undertaken in order to validate these findings.

Table 19 - Analytical Beam Results at Ultimate

Beam	Concrete Strain ϵ_c	Neutral Axis Position c mm (in)	Effective Stress in the Tendons after Losses MPa (ksi)	Top Tendon Strain ϵ_{pB}	Bottom Tendon Strain ϵ_{pB}	κ_m Bond Factor	Existing Substrate Strain $\epsilon_{bi}^{(1)}$	SRP Strain ϵ_{SRP}	M_n kN-m (kip-ft)	P_u kN (kip)	Failure Mode	$P_{u-Experimental} / P_{u-Analytical}$
DT-C	0.0010	21.08 (0.83)		0.012	0.0230	N/A *	N/A *	N/A *	393 (290)	337 (75.8)	Attainment of Limit Tendon Strain	0.98
DT-1	0.0006	34.8 (1.37)	1303 (189)	0.0053	0.0106	0.900		0.0149	454 (335)	389 (87.5)	Attainment of SRP	1.00
DT-2U	0.0006	37.3 (1.47)		0.0049	0.0099	0.842	-0.0001	0.0139	513 (380)	442 (99.4)	Effective Strain Limit	1.02

*N/A = Not Applicable

⁽¹⁾Determined from an elastic analysis considering only the self weight of the beams, at time of SRP installation

6.5 Conclusions

The following conclusions may be drawn from the field experimental program:

- SRP composite materials have shown to be effective in increasing the flexural capacity of the double-T PC beams.
- End anchors in the form of SRP U-wraps have shown to be effective by preventing a complete detachment, once debonding has occurred throughout the concrete-SRP interface.
- SRP is similar to FRP in terms of ease of installation, although self weight should not be ignored when selecting the resin system in overhead applications.
- Epoxy resin well behaved in bonding the steel tape to the concrete substrate.
- The analytical validation, using ACI 440 provisions has proven to be effective in anticipating the ultimate capacity, although further investigation in a controlled laboratory environment is need to properly calibrate the k_m bond factor.

7 REFERENCES

ACI 318-02, 2002: "Building Code Requirements for Structural Concrete and Commentary (318R-02)," Published by the American Concrete Institute, Farmington Hills, MI, pp. 443.

ACI 440.2R-02, 2002: "Guide for the Design and Construction of Externally Bonded FRP Systems for Strengthening Concrete Structures," Published by the American Concrete Institute, Farmington Hills, MI, pp. 45.

ASTM D 3039, 2002: "Test Method for Tensile Properties of Fiber Resin Composites" Published by the American Society for Testing and Materials, West Conshohocken, PA, pp. 13.

ASTM Standard D 790, Standard Test Methods for Flexural Properties of Unreinforced and Reinforced Plastics and Electrical Insulating Materials. Current edition approved on April 10, 2002.

Bisby, L.A., Kodur, V.K.R., and Green, M.F. "Performance in Fire of FP-Confined Reinforced Concrete Columns," Fourth International Conference on Advanced Composite Materials in Bridges and Structures - ACMBS-IV July 20-23, 2004 The Westin Hotel, Calgary, Alberta, Canada.

Ceroni, F., Pecce, M., Prota, A. and Manfredi, G, 2004, "Flexural Strengthening of RC Beams using Emerging Materials:Cracking Behavior", Proceedings of the International Conference FRP Composites in Civil Engineering - CICE 2004 - Seracino (Ed.), ISBN 90 5809 638 6, pp. 171-178.

Cosenza, E., and Pecce, M., 2001, "Shear and normal stresses interaction in coupled structural systems," ASCE Journal of Structural Engineering, V. 127, No. 1, pp. 84-88.

FIB Bulletin 14 (2001). "Design and use of externally bonded fibre reinforced polymer reinforcement (FRP EBR) for reinforced concrete structures, by 'EBR' working party of FIB TG 9.3, July 2001, 138 pp.

Gibson, RF. Principles of Composite Material Mechanics. McGraw-Hill, Inc., New York, NY, 1994.

Hardwire LLC, 2002, "What is Hardwire," www.hardwirellc.com, Pocomoke City, MD.

Mabey Bridge & Shore, Inc., www.mabey.com, Baltimore, MD.

Mapei, 2000, "World-wide Leader in Products for the Building Industry", <http://www.mapei.it>, Milan, Italy.

Nawy, G. E., "Prestressed Concrete", Prentice Hall, Upper Saddle River, NJ, 2002, 789 pp.

PCI (1999): "PCI Design Handbook: Precast and Prestressed Concrete", Published by the Precast/ Prestressed Concrete Institute, Chicago, IL.

Rizkalla, S. and Nanni, A. (2003) "Field Applications of FRP Reinforcement: Case Studies" ACI Special Publication 215, Published by the American Concrete Institute, Farmington Hills, MI.

Seible, F.; Priestley, M. J. N.; Hegemier, G. A.; and Innamorato, D., 1997, "Seismic Retrofit of RC Columns with Continuous Carbon Fiber Jackets," *Journal of Composites for Construction*, No. 1, pp. 52-62.

Shin, Y., and Lee, C., 2003, "Flexural Behaviour of Reinforced Concrete Beams Strengthened with Carbon Fiber-Reinforced Polymer Laminates at Different Levels of Sustaining Loads," *ACI Structural Journal*, V.100, No. 2, pp. 231-239.

Sika, 2005, "Sikadur 330 and Sika Top 121", www.sikausa.com, Lyndhurst, New Jersey.

Tashito, H., Tarui, T., Sasaki, S., Yoshie, A., Nishida, S., Ohashi, S., Nakamura, K., and Demachi, H., 1999, "Ultra High Tensile Strength Steel Cord," *Nippon Steel Technical Report* No. 80, Tokyo, Japan, pp. 38-43.

Teng, J.G., Chen, J.F., Smith, S.T., and Lam, L., 2001, *FRP Strengthened RC Structures*, John Wiley & Sons, Ltd, Chichester, England, pp. 245.

Todeschini, C., Bianchini, A, and Kesler, C. (1982) "Behavior of Concrete Columns Reinforced with High Strength Steels." *ACI Journal, Proceedings*, Vol. 61, No. 6, pp 701-716, November-December

Williams, B.K., Kodur, V.K.R., Bisby, L.A., and Green, M.F. "The Performance of FRP-Strengthened Concrete Slabs in Fire," *Fourth International Conference on Advanced Composite Materials in Bridges and Structures - ACMBS-IV* July 20-23, 2004 The Westin Hotel, Calgary, Alberta, Canada.